PALEOCEANOGRAPHY, VOL. 15, NO. 6, PAGES 570-592 DECEMBER 2000

Export production and carbonate dissolution in the central equatorial Pacific Ocean over the past 1 Myr

R. W. Murray,[1] C. Knowlton,[2] M. Leinen,[2,3] A. C. Mix,[4] and C. H. Polsky[1,5]

Abstract. In order to quantify changes in export production and carbonate dissolution over the past 1 Myr in the central equatorial Pacific Ocean we analyzed Ba, P, Al, Ti, and Ca in 1106 samples from five piston cores gathered from 5°S to 4°N at 140°W. We focused on Ba/Ti, Al/Ti, and P/Ti ratios as export proxies and employed areally integrated time slice as well as time series strategies. Carbonate maxima from 0-560 kyr are characterized by 15-30% greater export than carbonate minima. The increases in export fall on glacial $\delta^{18}O$ transitions rather than glacial maxima. From 560-800 kyr, overlapping with the mid-Pleistocene transition, there is a very large increase in total export yet no glacial-interglacial variability. The highest latitudes (5°S and 4°N) record minimal absolute export change from glacials to interglacials and yet record the most extreme minima in percent $CaCO_3$, indicating that carbonate records there are dominated by dissolution, whereas near the equator they are more influenced by changes in export.

1. Introduction

Much recent effort has gone toward answering an old paleoceanographic problem, namely, the cause of the pronounced cycles of calcium carbonate ($CaCO_3$) in Pleistocene sediments from the central equatorial Pacific Ocean. To briefly summarize a rich literature dating from their initial discovery [*Arrhenius*, 1952], the operation of two end-member processes, changes in dissolution and changes in export production, are thought to play a critical role in the formation of these cycles. While both processes are operating to some extent continuously with one or the other being more important at different locations in time and space, there is no consensus regarding the efforts to partition their relative importance, despite efforts focusing on the biogenic $CaCO_3$, opal, and organic carbon (C_{org}) components themselves [e.g., *Hays et al.*, 1969, 1976; *Adelseck and Anderson*, 1978; *Chuey et al.*, 1987; *Arrhenius*, 1988; *Lyle et al.*, 1988; *Pisias and Rea*, 1988; *Pedersen*, 1983; *Pedersen et al.*, 1988, 1991; *Rea et al.*, 1991; *Farrell and Prell*, 1989; *Herguera and Berger*, 1991, 1994; *Mix*, 1989; *Mix et al.*, 1991; *Loubere*, 1991, 1994, 1999; *Weber and Pisias*, 1999, and references therein], the dissolution record of the biogenic components [*Berger*, 1970, 1972, 1973, 1977; *Thompson and Saito*, 1974; *Berger and Herguera*, 1992; *Wu and Berger*, 1989; *Wei et al.*, 1994; *Weber et al.*, 1995; *LaMontagne et al.*, 1996, and references therein], chemical and mineralogical proxies of export production and nutrient uptake [*Goldberg and Arrhenius*, 1958; *Murray*, 1987; *Pedersen*, 1983; *Pedersen et al.*, 1988; *Lyle et al.*, 1992; *Murray et al.*, 1993, 1995; *Farrell et al.*, 1995; *Paytan et al.*, 1996, and references therein], and modeling results [*Archer*, 1991a, 1991b; *Oxburgh*, 1998; *Oxburgh and Broecker*, 1993; *Stephens and Kadko*, 1997; *Knowlton*, 1998, and references therein].

The recently concluded Joint Global Ocean Flux Study (JGOFS) in the equatorial Pacific Ocean provides new opportunities to answer this old problem. One of the main goals of this program was to examine the relation between the contemporary and paleoceanographic fluxes of material [*JGOFS*, 1990], and the large oceanographic database gathered along a meridional transect at 140°W longitude [*Murray*, 1995, 1996; *Murray et al.*, 1997] provides a terrific context within which to approach the problem. For example, integrating studies of meridional gradients in particle fluxes through the water column [e.g., *Honjo et al.*, 1995], phytodetritus and benthic fluxes [*Smith et al.*, 1996, 1997], sedimentary fluxes of trace metals and mineralogical proxies [e.g., *Murray and Leinen*, 1993, 1996; *Paytan et al.*, 1996], and dissolution [*McManus et al.*, 1995; *Hammond et al.*, 1996; *Berelson et al.*, 1997] in the modern ocean with paired study of the surface sediments and water column characteristics allows for the development of geochemical tools that can be applied down core for paleoceanographic studies.

In this paper we present results of inorganic chemical analysis of five piston cores gathered during the JGOFS equatorial Pacific program (Figure 1). These JGOFS cores were taken at different latitudes on a single meridional transect, thus allowing us to compare biogenic cyclicity, burial fluxes, and other parameters through the same latitudinal range as other JGOFS studies of the water column and surface sediment. We exploit this five-core database to examine export production and carbonate dissolution over the past one million years of Earth history.

[1]Department of Earth Sciences, Boston University, Boston, Massachusetts.
[2]Graduate School of Oceanography, University of Rhode Island, Narragansett
[3]On leave at Geosciences, National Science Foundation, Arlington, Virginia.
[4]Ocean Sciences, Oregon State University, Corvallis.
[5]Now at Department of Chemistry and Biochemistry, Arizona State University, Tempe.

Paper number 1999PA000457.
0883-8305/00/1999PA000457$12.00

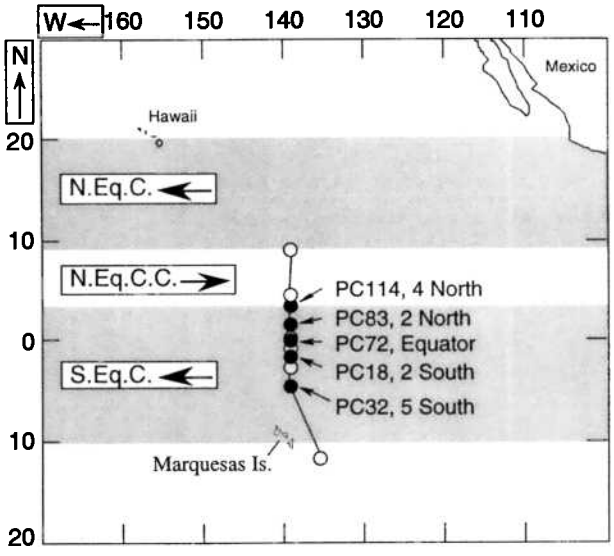

Figure 1. Map of the central equatorial Pacific Ocean showing the Joint Global Ocean Flux Study (JGOFS) transect along 140°W JGOFS transect. Solid circles show location of the five piston cores; solid and open circles show locations of surface sediment samples. Representative positions of oceanic currents are marked as follows: N.Eq.C., North Equatorial Current; N.Eq.C.C., North Equatorial Countercurrent; S.Eq.C., South Equatorial Current. Position of Marquesas Islands (9.5°S, 140°W) is schematically indicated.

2. Chemical Tracers of Export Production

2.1. Selection of Proxies

As with *Murray et al.* [2000], we use elemental ratios based on three different chemical proxies of export production, namely, Ba, Al_{excess}, and P. By studying elemental ratios and not absolute accumulation rates we avoid potential age model artifacts associated with changes in sedimentation rate. In using Ba as a proxy we exploit previous observations that demonstrate a strong tie between the formation of the mineral barite ($BaSO_4$) in the water column and export production [*Goldberg and Arrhenius*, 1958; *Dehairs et al.*, 1980, 1987, 1990, 1992; *Bishop*, 1988; *Stroobants et al.*, 1991; *Dymond et al.*, 1992; *Francois et al.*, 1995]. Our strategy involving Al_{excess}, manifested as the Al/Ti ratio, takes advantage of previous observations relating an Al_{excess} component (i.e., not tied to an aluminosilicate fraction) to biogenic fluxes through the water column and to the seafloor [*Murray et al.*, 1993; *Murray and Leinen*, 1996; *Dymond et al.*, 1997; *Banakar et al.*, 1998]. Such use of Al/Ti is only appropriate in sediments such as these in the equatorial Pacific that contain very small concentrations of terrigenous matter [e.g., *Yarincik et al*, 2000]. In using P we rely on previous observations correlating P distributions in marine sediments to productivity in the overlying water [*Froelich et al.*, 1982; *Filippelli and Delaney*, 1992, 1995, 1996; *Delaney*, 1998, and references therein]. While recognizing that no single proxy is a "magic bullet," we capitilize on the strength that each of these proxies traces a slightly different aspect of export production, and thus by looking at the three in unison we minimize artifacts associated with any single one.

Each proxy has specific limitations that need to be heeded. The analysis of elemental Ba in bulk sediment is itself performed as a proxy for a mineralogical measurement of the mineral barite [e.g., *Paytan et al.*, 1996]. Measuring Ba, instead of barite, causes a loss of information because Ba is not exclusively associated with barite either in the water column (where up to 40% of the total Ba inventory may not be contained in barite [e.g., *Dymond et al.*, 1992]) or in the buried sediments [e.g., *Schroeder et al.*, 1997]. Other issues are well summarized by *McManus et al.* [1998, 1999]. For Al_{excess}, observations from equatorial Pacific sediment [*Murray et al.*, 1993; *Murray and Leinen*, 1996] and from sediment in the Indian Ocean [*Banakar et al.*, 1998] indicate a non-particle specific association between Al_{excess} and the bulk particle flux and organic matter. These sedimentary observations are consistent with the understanding of the scavenged behavior of Al in the water column [e.g., *Orians and Bruland*, 1986; *Moran and Moore*, 1988, 1989] and experimental studies of the uptake of Al [e.g., *Moran and Moore*, 1992]. However, statistical modeling of sediment trap data suggests an important role of biogenic opal [*Dymond et al.*, 1997]. Thus, while Al/Ti is responding to export production in this environment, it remains unclear whether it is tracing bulk particle flux or the export of a specific component (e.g., diatoms). Finally, the diagenetically reactive nature of P [*Froelich et al.*, 1982; *Filippelli and Delaney*, 1995, 1996; *Delaney*, 1998] means that absolute concentrations of P (and therefore ratios such as P/Ti) may be affected by diagenetic losses of labile P. These diagenetic resetting(s) may be not be linear in time and space.

We interpret our data set within the tolerance of these uncertainties. Limitations such as these are not unique to trace element proxies and do not overly handicap our interpretations. We feel our approach is valid given (1) the power of working with a very large data set spanning a meridional range and multiple glacial-interglacial cycles, (2) that we are working with three different proxies that each respond to a different aspect of upper water column biogeochemical cycling, and (3) that we are considering these proxies as a combined data set, allowing internal checks on our conclusions.

2.2 Proxy Normalization to Titanium Concentration

Studying the down core distribution of the concentration of either Ba, Al, or P would largely only record dilution by the dominant component in the sediment, which in this case is $CaCO_3$. In order to account for dilution we normalized our elemental data to the concentration of Ti in the same sample. This allows a more accurate comparison of elemental changes because ratios of two variables are unaffected by dilution caused by a third. While it is common to use Al for normalization, in sediments that have a large Al_{excess} component this yields an erroneous result. Although use of Ti also assumes that all Ti is tied to the lattices of terrigenous phases, a portion of the Ti may also be adsorbed, given the particle reactive nature of Ti in seawater [e.g., *Orians et al.*, 1990]. Because the predominant detrital source to sediments in this region is eolian material [*Chuey et al.*, 1987] and because there are only slight differences in the Ti

concentrations in the potential sources of this dust (e.g., average shale, loess, and upper continental crust) [*Murray and Leinen*, 1996], it is unlikely that we are inadvertantly creating an artifact due to provenance changes through time. The above set of conditions, however, applies only to where ocean island basalts (OIB) are not providing detrital material because such material is enriched in Ti [e.g., *Gill*, 1981]. Owing to this enrichment a provenance signal from an OIB source is clearly recognized in the chemical data, as shown below in the context of our cores taken in the Southern Hemisphere, relatively close to the Marquesas Islands.

Another important consideration when interpreting elemental ratios is autocorrelation. In a core with constant concentrations of Ba, for example, variations in the amount of Ti will produce changes in Ba/Ti. Although the relative amount of Ba (i.e., with respect to Ti) will be varying in this case, fluctuations in Ti could lead to the erroneous interpretation that the absolute flux of Ba is changing. In this situation we would expect a correlation between Ba/Ti, Al/Ti, and P/Ti, and this autocorrelation would reflect the commonality of mutual division by Ti instead of the independent aspects of paleoexport. One can test for autocorrelation, however, by considering the Ba/Ti ratio in a representative average shale (e.g., Ba/Ti = 0.11 g/g in Post Archean Average Shale (PAAS) of *Taylor and McLennan* [1985]). Any variance in [Ba] (=[$Ba_{maximum}$] - [$Ba_{minimum}$]) that is greater than approximately one tenth the variance in [Ti] indicates that the bulk ratio is recording variability in the total Ba inventory that is greater than can be explained by changing only the relative input of terrigenous Ti. From the data below it will become clear that this and analogous arguments hold for Al/Ti and P/Ti as well. For Al/Ti in cores PC32 and PC18, in the Southern Hemisphere, this comparison must be used with ratios of Marquesas Islands material, rather than PAAS, for reasons discussed below.

3. Proxy Response Across Surface Sediment Transect

Murray et al. [2000] summarize data on the three proxies and how they relate to other parameters linked to export production in surface sediment along the cross-equator meridional transect (Figure 2). Because we rely on these surface distributions to justify the down core use of these proxies, we reiterate here several observations. First, as noted on a similar transect at 135°W [*Murray and Leinen*, 1993], the meridional profile of the concentration of $CaCO_3$ displays a stepped plateau of elevated values from ~5°S to 5°N (Figure 2). In contrast to this presence/absence pattern of $CaCO_3$ concentration, the patterns of total productivity in the overlying water, seafloor phytodetritus [*Smith et al.*, 1996], bulk sedimentary accumulation rate [*Murray and Leinen*, 1993, 1996], and the elemental ratios of Al/Ti [*Murray et al.*, 1993; *Murray and Leinen*, 1996], Ba/Ti [*Schroeder et al.*, 1997], and P/Ti [*Murray et al.*, 2000] record a sharply peaked profile, with maxima centered at 1°S or at the equator (Figure 2). As discussed later, there is a strongly linear relationship between the proxies and productivity of the surface water.

Each of these V-shaped profiles is markedly different from the stepped profile of percent $CaCO_3$, and the close correlation

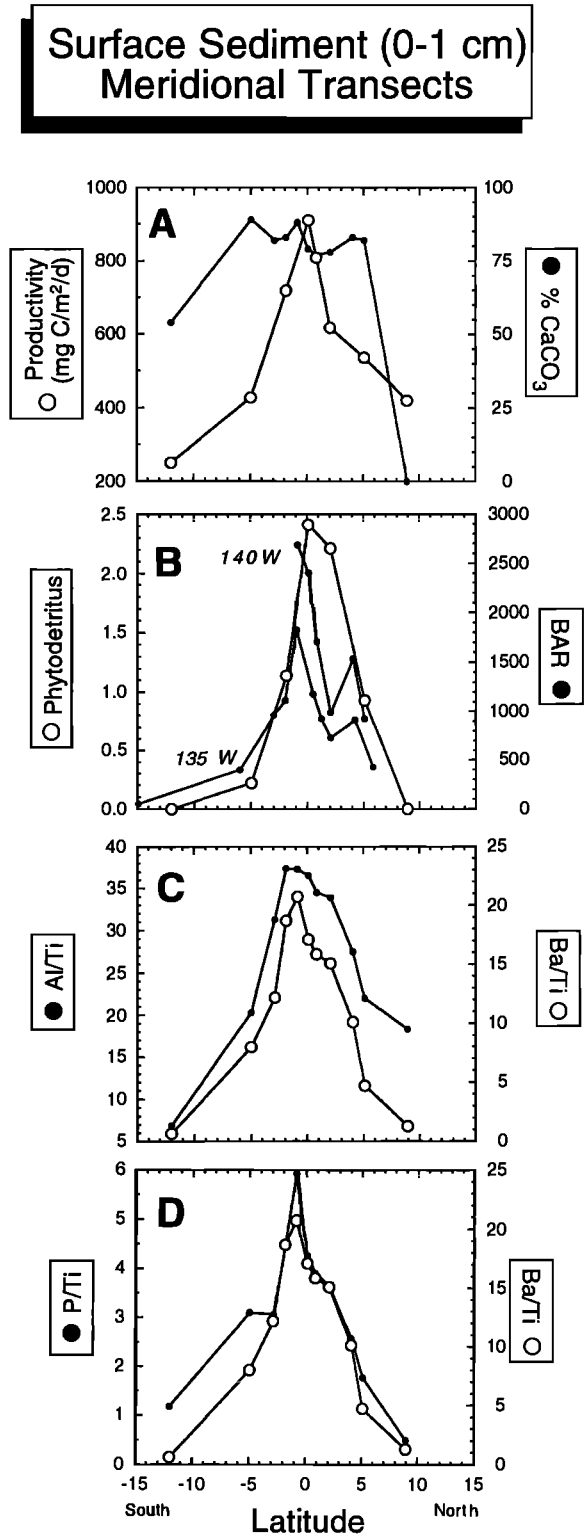

Figure 2. Meridional profiles at 140°W (a) Total productivity (average values, from sources in *Paytan et al.* [1996]) and the concentration of $CaCO_3$ (wt %) in the surface sediment. (b) Abundance of phytodetritus laying on the seafloor [*Smith et al.*, 1996] and the bulk accumulation rate (BAR) of the sediment (along 135°W from *Murray and Leinen* [1993], along 140°W from *Murray and Leinen* [1996]). (c) Bulk Al/Ti and Ba/Ti in surface sediment (from *Murray and Leinen* [1996] and *Schroeder et al.* [1997]). (d) Bulk Ba/Ti and P/Ti in surface sediment [from *Murray et al.*, 2000].

between the proxies, water column parameters, and accumulation rates strongly indicates that the proxies are recording biologic and water column removal/transport processes rather than sediment composition or earliest diagenesis. The rate of decrease away from the equator is significantly less in the Northern Hemisphere than in the Southern. The accumulation rates of the individual biogenic components also record this pattern [*Murray and Leinen*, 1993]. The low values of the Ti-normalized ratios in the southernmost sites of the transect are lower than those found in average shale, recording Ti-rich OIB input from the Marquesas Islands [*Murray and Leinen*, 1996]. Although the multicores taken along the surface transect recover the uppermost 0-1 cm interval (including the most recent "fluff layer"), owing to the varying sedimentation rates along the transect this uppermost 1 cm averages the past ~0.3 kyr at the lowest latitudes to 1 kyr at higher latitudes [*Murray and Leinen*, 1993, 1996].

4. Stratigraphy and Methodologies

4.1. Piston Cores

The piston cores used in this study (Figure 1, Table 1) were selected to sample key geographic positions along the meridional gradients in modern export production. Throughout this paper we abbreviate the full core denomination (e.g., core TT013-PC114 for the core at 4°N) using only the "PC" number (e.g., PC114). The cores are curated at the Graduate School of Oceanography, University of Rhode Island.

4.2. Age Models and Stratigraphy

The age models for cores PC18 and PC72 were determined by correlating the SPECMAP stack of *Imbrie et al.* [1984] to the $\delta^{18}O$ analyses of *Cibicides wuellerstorfi*. Isotopic analysis and development of the isotopic age models was performed at Oregon State University. For cores PC32, PC83, and PC114 the age models were determined at the University of Rhode Island by correlation of the $CaCO_3$ concentration profile to the isotopically constrained $CaCO_3$ concentration records of PC18 and PC72 [*Knowlton*, 1998]. On the basis of these age models and the sampling interval selected for this study it is apparent that the piston cores provide full coverage over the past 783-1045 kyr, with a temporal resolution of 3-6 kyr per sample (Table 1).

In this paper we take a "time slice" and a "time series" approach to the data set. For the time slices (Table 2) we have selected the midpoint, in kiloyears, of each carbonate stage (B2, B3, etc.), following the nomenclature but not the exact ages outlined in *Farrell and Prell* [1989] and *Snoeckx and Rea* [1994, and references therein]. The exact timing of these midpoints were selected on the basis of the percent $CaCO_3$ records in PC18 and PC72, the two cores in our study for which we have an isotopically determined age model. Using correlations based on percent $CaCO_3$ [*Knowlton*, 1998], these carbonate stages were extended to the higher latitude cores. For core PC32 some of these midpoints are not true temporal midpoints, given the low resolution of the record, but they are well correlated graphically to the maxima and minima in percent $CaCO_3$ of the other records.

In the discussions of the variations in elemental ratios we took numerical averages of values during the different carbonate stages (Table 2) and where possible avoided sampling the transitions into and out of the carbonate minima. For the carbonate maxima, these averages were determined with as many as 25 data points (e.g., stage B10 in core PC72). For the sharply defined carbonate minima, these averages were determined with as few as two data points (e.g., stage B9 in core PC72). In the very oldest records, sometimes only one data point exists for a given carbonate minimum. We chose to compare a given carbonate maximum with the immediately younger carbonate minimum rather than with the older one because it enables comparison of the last maximum to the surface sediment. We conducted sensitivity tests of our point selection schemes and determined that changes in the point selection make no difference in the overall patterns we observe. One of the strengths of the data set lies in its size; the selection of alternative data points (or older/younger comparisons versus younger/older) does not alter the results.

For the "time series" approach we investigate the record provided by core PC72, and use the temporal relationships between the elemental chemical ratios, percent $CaCO_3$, and $\delta^{18}O$ to constrain the changes through time in export production, carbonate burial, and glacial-interglacial climate state. We have chosen this core because it has the highest resolution combined with the longest record of our sample set (Table 1) and has been investigated for a variety of other studies [e.g., *Murray et al.*, 1995; *Marcantonio et al.*, 1995, 1996; *Paytan et al.*, 1996]. Thus the time series analyses we perform here will be applicable to these other projects as well. We used the ARAND software package (Brown University) to

Table 1. Piston Cores, 140°W JGOFS Transect

Core TT013-	Lat., deg	Long., deg	Water Depth, m	Age Model	Analyzed Length, cm	Age at Base, kyr	Sed. Rate, cm/kyr	Sampling Interval, cm	Resolution, kyr	Number of Samples
PC114	4.04°N	139.85°W	4432	carbonate	790	939	0.8	5.0	6 ± 4	153
PC83	2.07°N	140.15°W	4414	carbonate	1035	1037	1.0	5.0	5 ± 2	202
PC72	0.11°N	139.40°W	4298	isotopic	1595	1045	1.5	5.0	3 ± 2	314
PC18	1.84°S	139.71°W	4354	isotopic	1290	783	1.6	5.0	3 ± 2	242
PC32	4.96°S	139.74°W	4236	carbonate	500	938	0.5	2.5	5 ± 3	195

"Lat." indicates "Latitude", "Long." indicates "Longitude", "Sed." indicates "Sedimentation".

Table 2. Ages of Carbonate Stages and Number of Samples Per Stage, Per Core

Stage	Midpoint, kyr	Age of Stage, kyr				
		PC32; 5°S	PC18; 2°S	PC72; Equator	PC83; 2°N	PC114; 4°N
B2	30	20 8 - 54.0 (n = 7)	15.8 - 50.6 (n = 13)	17.4 - 57 4 (n = 16)	30.1 - 57 5 (n = 5)	26 6 - 56 5 (n = 9)
B3	103	87.3 - 109.9 (n = 7)	67 7 - 110.3 (n = 9)	68.4 - 116.0 (n = 13)	77.9 - 109 1 (n = 4)	71.6 - 113 4 (n = 5)
B4	155	125.0 - 155.3 (n = 11)	121.6 - 163.4 (n = 15)	125.5 - 166.0 (n = 18)	122.2 - 151 2 (n = 6)	121.7 - 152.5 (n = 6)
B5	182	176.5 - 188.6 (n = 4)	175.5 - 184.8 (n = 3)	177.1 - 185.9 (n = 4)	166 9 - 189 2 (n = 5)	167 6 - 191 0 (n = 5)
B6	234	200.9 - 237.7 (n = 7)	194 0 - 251 0 (n = 12)	203 5 - 255.9 (n = 17)	211.8 - 237 2 (n = 3)	233 3 - 262 2 (n = 4)
B7	272	274.5 - 283 3 (n = 2)	269.0 - 273.1 (n = 3)	269.6 - 274.5 (n = 3)	265.2 - 274 7 (n = 2)	268 0 - 277 9 (n = 3)
B8	327	335.8 - 362.1 (n = 4)	322 3 - 360 8 (n = 13)	315.6 - 355.7 (n = 16)	311.6 - 337 4 (n = 5)	326 0 - 342 0 (n = 3)
B9	399	379.9 - 398.6 (n = 4)	391 7 - 404.9 (n = 4)	395.9 - 398.6 (n = 2)	387.2 - 401 9 (n = 3)	374.1 - 395 8 (n = 5)
B10	442	411.4 - 456.5 (n = 8)	423.8 - 461.6 (n = 17)	407.5 - 458.5 (n = 25)	406.1 - 459 0 (n = 13)	403.2 - 464 4 (n = 6)
B11	476	475.8 - 482 4 (n = 3)	475 5 - 479.1 (n = 3)	473.6 - 478.2 (n = 3)	470 4 - 477.2 (n = 3)	473.9 - 481.4 (n = 3)
B12	535	509.0 - 533.9 (n = 4)	507.5 - 552 5 (n = 15)	509.5 - 550.5 (n = 13)	506.4 - 536.9 (n = 7)	506.0 - 533 9 (n = 5)
B13	576	567.2 - 585 5 (n = 5)	570 0 - 575.1 (n = 2)	575.5 - 577.4 (n = 2)	564.8 - 573.4 (n = 3)	564.4 - 574 6 (n = 2)
B14	652	612.4 - 652.6 (n = 12)	640.3 - 661.2 (n = 12)	636 1 - 668.5 (n = 11)	636.1 - 667 5 (n = 10)	636 7 - 675 1 (n = 8)
B15	682	676.1 - 690.4 (n = 6)	684 0 - 685 0 (n = 2)	676 1 - 687.5 (n = 6)	677 9 - 684 9 (n = 3)	684.0 - 696 4 (n = 4)
B16	738	700.7 - 734.8 (n = 11)	706 3 - 750 9 (n = 16)	709.3 - 767.3 (n = 15)	696 4 - 754.4 (n = 16)	705 4 - 748.0 (n = 10)
B17	778	779.2 - 785.4 (n = 2)	765 8 - 769.4 (n = 2)	777.3 - 779.2 (n = 2)	769.6 - 777 3 (n = 3)	777 5 - 789 3 (n = 3)
M0	798	791.6 - 822 8 (n = 6)	779 7 - 783 1 (n = 2)	782.8 - 812.1 (n = 11)	786.7 - 810.2 (n = 6)	801 2 - 813 0 (n = 4)
M1	842	841.4 - 857.2 (n = 4)		837 3 - 847 7 (n = 3)	843 0 - 852 2 (n = 3)	836 6 - 854 3 (n = 3)
M2	908	874.4 - 914.6 (n = 8)		889 4 - 926 0 (n = 7)	865.7 - 919.9 (n = 13)	866 I - 929 7 (n = 10)
M3	939	938.0 (n = 1)		938.0 - 940 6 (n = 2)	933.5 - 942.8 (n = 3)	937 7 - 939.4 (n = 2)
M4	990			951.0 - 1028.4 (n = 11)	971.9 - 1020.4 (n = 11)	
M5	1035			1034 9 (n = 1)	1034 9 (n = 1)	

Midpoints (kyr) of stages B2 through B13, as defined in core PC72, are identical to those given by *Knowlton* [1998], except for stages B7 and B13, for which ages here are 3 kyr (1-2 data points) younger than *Knowlton* [1998] Midpoints for stages B14 through M5 in this data set are defined here.

perform spectral and cross-spectral analyses on the data set. For reasons that will become clear below we have divided the spectral study into two different periods. The first comprises the record from 0 to 565 kyr (to the marine isotopic stage (MIS) 14/15 boundary [*Imbrie et al.*, 1984]), while the second comprises the record from 565 to 1044 kyr. We have also performed the time series analysis on the entire 0-1044 kyr record.

4.3. Inductively Coupled Plasma Emission Spectrometry (ICP-ES)

The concentrations of Ba, Al, Ti, and P in 1106 samples were measured by ICP-ES at Boston University, using a Jobin-Yvon JY24 sequential spectrometer. For core PC32, Ca was also measured. Procedures for the combined HF-HNO_3-HCl-H_2O_2 dissolution methods, ICP-ES analyses, and data reduction are collectively described by *Murray et al.* [1995, 2000], *Murray and Leinen* [1996], and *Schroeder et al.* [1997].

Precision was quantified by multiple analyses (upward of 10 measurements per replicate sample from a given core and from the powder-weighing step onward) of natural JGOFS sediments included in every analytical batch. Precision of the measurements is 4% of the measured values for Ba and Al, 3% of the measured value for Ti (and Ca in PC32), and 23% of the measured value for P. Given the low absolute concentrations of these elements in the high-carbonate samples, these percentages result from relatively low uncertainties in terms of parts per million (ppm) units with typical "concentration ± uncertainty" absolute values being Ba = 1142 ± 50 ppm, Al = 2998 ± 126 ppm, P = 241 ± 51 ppm, and Ti = 96 ± 3 ppm. The higher uncertainty in the measurement of P reflects that an older ICP-ES in use at Boston University at the time of these measurements was an air path spectrometer, and thus the wavelength used for the measurement of P had a high interference. Even with this higher uncertainty for P, however, the changes we observe in P distributions in the cores (commonly on the order of 200-300%) greatly exceed the precision of the measurement and thus can confidentally be interpreted as being signal rather than noise. Also, as discussed below in the context of analytical accuracy, measurements of P in a Standard Reference Material (SRM) are within 10% of the accepted value.

Replicate calculations of the elemental ratios in these same JGOFS natural samples yield a precision of the ratios of Ba/Ti = 12.6 ± 0.4 (3% of the measured value); Al/Ti = 32.1 ± 1.4 (4%); and, P/Ti = 2.9 ± 0.5 (22%). As discussed by *Murray and Leinen* [1996], precision of these ratios is better than the sum of the precision of the individual elements since the processes that introduce uncertainty, such as weighing and dilution errors, act in the same direction for each element. Samples were prepared and analyzed in different random orders so as to not introduce artifical down core trends. Although these estimates of precision indicate a well-constrained data set, they are worst-case values because they are based on replicate analyses tracking the 25-30 batches of samples prepared and analyzed over 2-3 years. Many variables that naturally occur in a laboratory over a several year period (e.g., multiple sets of calibration standards and different technicians) are quantified by these estimates.

Accuracy was ensured by multiple analyses of the SRM NIST-1C (an argillaceous limestone) provided by the National Institute of Standards and Technology (NIST) of the U.S. Government. Accuracy for Al and Ti, including a study of the effect of the high concentrations of $CaCO_3$, was constrained as described by *Murray and Leinen* [1996], and accuracy for Ba was constrained as described by *Schroeder et al.* [1997]. Accuracy for P is within precision of the measurement, and is within 10% of the accepted value. This provides additional information that our estimate of the P precision (~20% of the measured value) is in fact a worst-case approximation.

4.4. Determination of the Abundance of $CaCO_3$ and Terrigenous Matter

The abundance of $CaCO_3$ in all cores except for PC32 was quantified using standard coulometric techniques at the University of Rhode Island. Precision, based on replicate measurements of natural samples, is 0.1% of the measured value, and accuracy was confirmed by comparison to a pure $CaCO_3$ standard [*Knowlton*, 1998]. For core PC32 the concentration of $CaCO_3$ was determined using a normative calculation that assumes all the Ti in a given sample is contained within a detrital phase, according to

$$\%CaCO_3 = \{\%Ca_{total} - \%[Ti_{total} \times (Ca_{shale}/Ti_{shale})]\}/0.4 \quad (1)$$

with Ca being determined by ICP-ES at Boston University. We have selected the concentration of Ti in PAAS [*Taylor and McLennan*, 1985] as the reference concentration for Ti_{shale}. The correction for terrigenous Ca in (1) amounts to only a maximum of 1-2 wt % $CaCO_3$ but is nonetheless performed for completeness. Although $CaCO_3$ is determined differently in core PC32 than in the other cores, there is no significant contrast in down core pattern of the two methods, based on comparative calculations using numerous samples where we have both coulometric and normative data.

The abundance of terrigenous matter is calculated from

$$\%terrigenous = 100\ (Ti_{total} / Ti_{PAAS}) \quad (2)$$

While there may be situations where such usage of Ti is not appropriate (e.g., ash layers or near the Marquesas Islands), this calculation provides a baseline of terrigenous abundance that allows intercore comparisons. As will become clear, in fact, this use of Ti readily identifies those intervals where nonshaley-type material is included in the nonbiogenic component, for Ti tends to be greatly enriched in these materials, and thus their signal is amplified.

5. Results and Preliminary Discussion

5.1. General Observations

Concentration data are provided in Appendices 1-5, which may be accessed through the World Data Center-A for Paleoceanography or from the senior author[1]. Information on the age models and temporal resolution is provided in Table 1. An overall summary of the data set is provided in Table 3 and

[1]Appendices 1-5 are available electronically at World Data Center-A for Paleoceanography, NOAA/NGDC, 325 Broadway, Boulder, CO 80303 (e-mail: paleo@noaa.ngdc.gov; URL: http://www.noaa.ngdc.gov/paleo).

Table 3. Data Summaries, Piston Cores TT013-, 140°W JGOFS Transect

Data Type	Parameter	PC32, 5°S	PC18, 2°S	PC72, Equator	PC83, 2°N	PC114, 4°N
Percent carbonate	average	83.4	87.9	86.0	83.2	79.3
Percent carbonate	standard deviation	11.6	5.2	7.0	8.5	12.5
Percent carbonate	minimum	47.3	67.3	58.2	52.8	38.7
Percent carbonate	maximum	100.0	94.9	96.5	93.4	93.6
Percent terrigenous	average	8.4	1.8	1.5	2.4	4.5
Percent terrigenous	standard deviation	7.1	1.9	1.1	1.7	3.5
Percent terrigenous	minimum	0.5	0.3	0.3	0.5	0.6
Percent terrigenous	maximum	32.0	16.7	5.8	7.6	15.0
Ba, ppm	average	1549	994	1399	1720	2027
Ba, ppm	standard deviation	999	489	791	1057	1395
Ba, ppm	minimum	244	282	419	489	509
Ba, ppm	maximum	4326	2938	4851	4973	6586
Ba, ppm	maximum minus minimum	4082	2656	4432	4484	6078
Al, ppm	average	6980	2442	3214	4372	7158
Al, ppm	standard deviation	4987	1506	2187	2979	5326
Al, ppm	minimum	968	328	701	1047	1215
Al, ppm	maximum	21390	8443	12429	13515	22287
Al, ppm	maximum minus minimum	20421	8115	11728	12469	21072
P, ppm	average	517	249	344	260	219
P, ppm	standard deviation	359	79	132	159	110
P, ppm	minimum	72	89	75	31	58
P, ppm	maximum	2070	579	971	868	598
P, ppm	maximum minus minimum	1998	490	897	837	540
Ti, ppm	average	502	105	90	144	270
Ti, ppm	standard deviation	428	115	64	103	212
Ti, ppm	minimum	28	18	18	30	37
Ti, ppm	maximum	1916	999	350	457	897
Ti, ppm	maximum minus minimum	1888	980	333	428	859
Ba/Ti, g/g	average	4.4	13.0	17.0	13.0	8.5
Ba/Ti, g/g	standard deviation	2.3	4.6	3.4	2.6	2.1
Ba/Ti, g/g	minimum	1.9	0.5	5.7	7.2	5.0
Ba/Ti, g/g	maximum	13.0	24.3	30.3	20.3	14 9
Al/Ti, g/g	average	16.8	29.2	36.7	31.3	27.6
Al/Ti, g/g	standard deviation	4.9	7.9	3.9	3.0	2.1
Al/Ti, g/g	minimum	10.7	0.6	10.3	20.8	23.1
Al/Ti, g/g	maximum	35.5	43.0	52.7	39.7	33.8
P/Ti, g/g	average	1.4	3.6	4.6	2.3	1.1
P/Ti, g/g	standard deviation	1.2	1.8	1.5	1.4	0.6
P/Ti, g/g	minimum	0.3	0.3	1.4	0.3	0.4
P/Ti, g/g	maximum	8.3	11.4	8.8	6.9	3.4

Data overspecified for calculation purposes. See text for true analytical precision.

in Figure 3. For each of the five parameters discussed in this paper (percent $CaCO_3$, percent terrigenous, Ba/Ti, Al/Ti, and P/Ti) we have determined the average value (± standard deviation) in each core as well as the minimum and maximum value.

The average concentration of $CaCO_3$ is high, ranging from an average of 79 wt % at 4°N to 88 wt % at 2°S. The concentration at 2°S is essentially identical to that at the equator. The latitudinal gradient in surface sediment percent $CaCO_3$ sampled by these cores is such that they are entirely from within the high-$CaCO_3$ region (Figure 3). Therefore, the average concentration of $CaCO_3$ as well as the highest values (in each core) also appear uniformly high and generally mimic the surface sediment profile (Figure 3a). The meridional

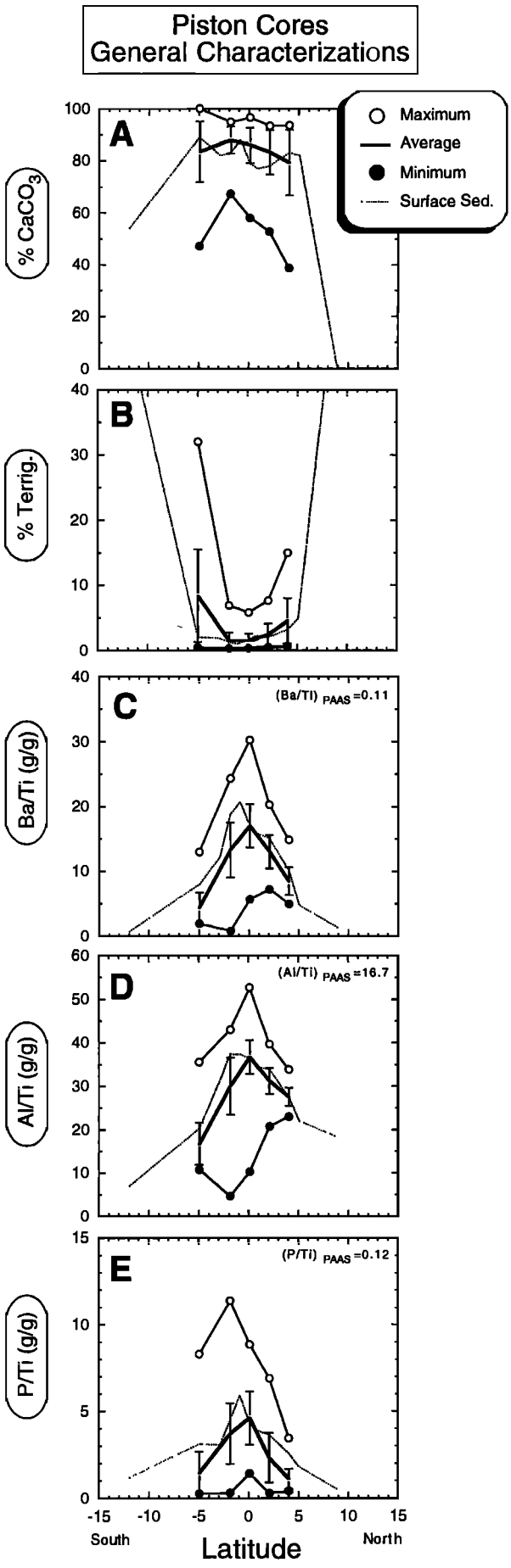

gradient of the minimum values of $CaCO_3$, however, displays a sharp peak at 2°S, such that the minimum values at the higher latitudes are much lower than the minimum value nearest the equator. This reflects that the carbonate minima at the higher latitudes decrease to much lower percent $CaCO_3$ values than the same minima at the lower latitudes.

The average concentration of terrigenous material is uniformly low, ranging from ~1 wt % at 2°S and the equator and up to 4-8 wt % at the higher latitudes (Figure 3b). Because this concentration is controlled by dilution of the terrigenous material by $CaCO_3$, the gradient in maximum terrigenous wt % also shows the sharp peak at the lowest latitudes (inverted, in this case, owing to dilution).

The distributions of the summary values of the three proxies display many commonalities (Figure 3c-3e). First, all patterns display the sharply peaked profile, not the stepped profile of $CaCO_3$. Second, the maximum values are consistently greater than the surface sediment. Third, the values of the proxies in the lower latitudes are consistently greater than the detrital averages. Fourth, the profiles of the minimum values appear different than the profiles of the averages or the maximum values. This is due in part to the presence of ash-rich intervals, as recorded by the Ti data, and will not be discussed.

5.2. Piston Core Summary: Five Cores

We present here a summary of the individual piston cores, emphasizing their similarities and contrasts. Although there is a wealth of information in each core, description of each one is avoided for brevity. In Figures 4-8, the axes on each plot are scaled to show the maximum variation in a given parameter, while in Figure 9 all cores are plotted at a common scale. We will present time series analyses of the PC72 record later in this paper, and in the following passages use of the term "cyclicity" is meant only to informally describe graphically visual repetitive increases and decreases in a given record. Collectively, the data for each core indicates the following:

1. Despite the poorer resolution of the off-axis cores (e.g., PC32 and PC114), the general patterns of percent $CaCO_3$ varying with time are apparent at all latitudes. The average concentrations of percent $CaCO_3$ are greatest at 2°S and at the equator, with the deepest minima appearing in the off-axis cores (PC32 and PC114). Carbonate minima at least as old as B11 (at 2°S) and stage M4 (or perhaps M5, at 2°N) are recognizable.

2. Superimposed upon the 100 kyr cyclicity in the percent $CaCO_3$ records is a longer period cycle (lasting 500-600 kyr) centered on carbonate stages B14-B16. This is particularly developed in PC32 (5°S) but is observable to some extent in all cores (e.g., in PC114 it is defined most clearly by variation in the minima in percent $CaCO_3$). Excluding the concentrations in the minima, percent $CaCO_3$ concentrations are higher than in surface sediment at the same latitude at 2°S and the equator, are approximately the same at 2°N, and are

Figure 3. Meridional transects of the maximum, average, and minimum values of percent $CaCO_3$ (wt %), percent terrigenous matter (wt %), and the three paleoproductivity proxies (g/g) in each core. Values of each parameter in the surface sediment (Figure 2) are also shown. For the paleoexport proxies, values in an average shale (PAAS) [*Taylor and McLennan*, 1985] are shown in each panel for comparison.

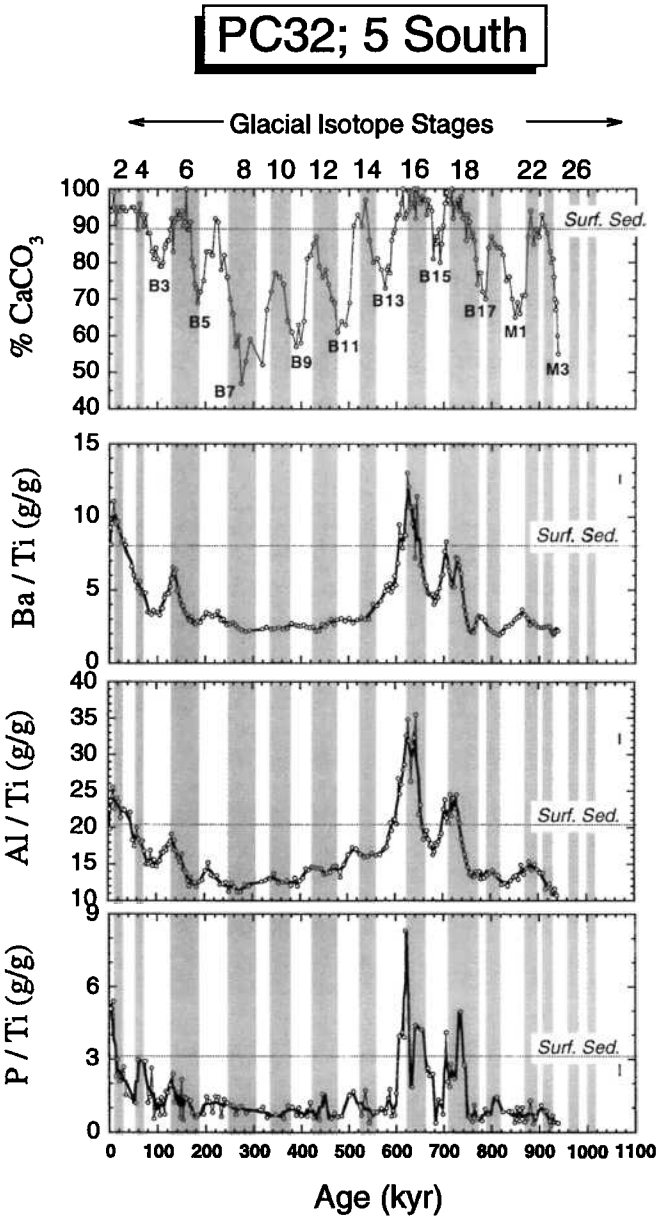

Figure 4. Age profiles of percent $CaCO_3$ (wt %) and the chemical proxies (g/g) in core PC32, located at 5°S. Glacial marine isotope stages (shaded) are from *Imbrie et al.* [1984]. Carbonate minima stages are from *Farrell and Prell* [1989] and *Snoeckx and Rea* [1994, and references therein]. In each panel the value of the given parameter in surface sediment at this latitude (Figure 2) is shown by the dashed line. For the chemical proxies, analytical precision is shown by the vertical bar to the far right in each panel. Thick line connecting points is a three-point running average.

significantly less than in surface sediment at 5°S and 4°N. The minima in percent $CaCO_3$ from the Holocene back to B11 is commonly a much smaller value than the minima in percent $CaCO_3$ from the older B13 to B17. The percent $CaCO_3$ minima are more deeply incised (reach lower values, on the order of ~40 wt %) in the off-axis cores compared to in the lower-latitude cores (with minima of the order of 55-60 wt % $CaCO_3$).

3. Down core profiles of Ba/Ti, Al/Ti, and P/Ti are closely correlative and generally very smooth. Nearest to the equator the proxies display slightly noiser records than in the off-axis cores, reflecting in part the greater sample resolution (Table 1).

4. There is strong 100 kyr cyclicity from 0 to ~560 kyr.

5. From 560 to 800 kyr, a period which broadly coincides with the mid-Pleistocene climate transition (MPT), there is a

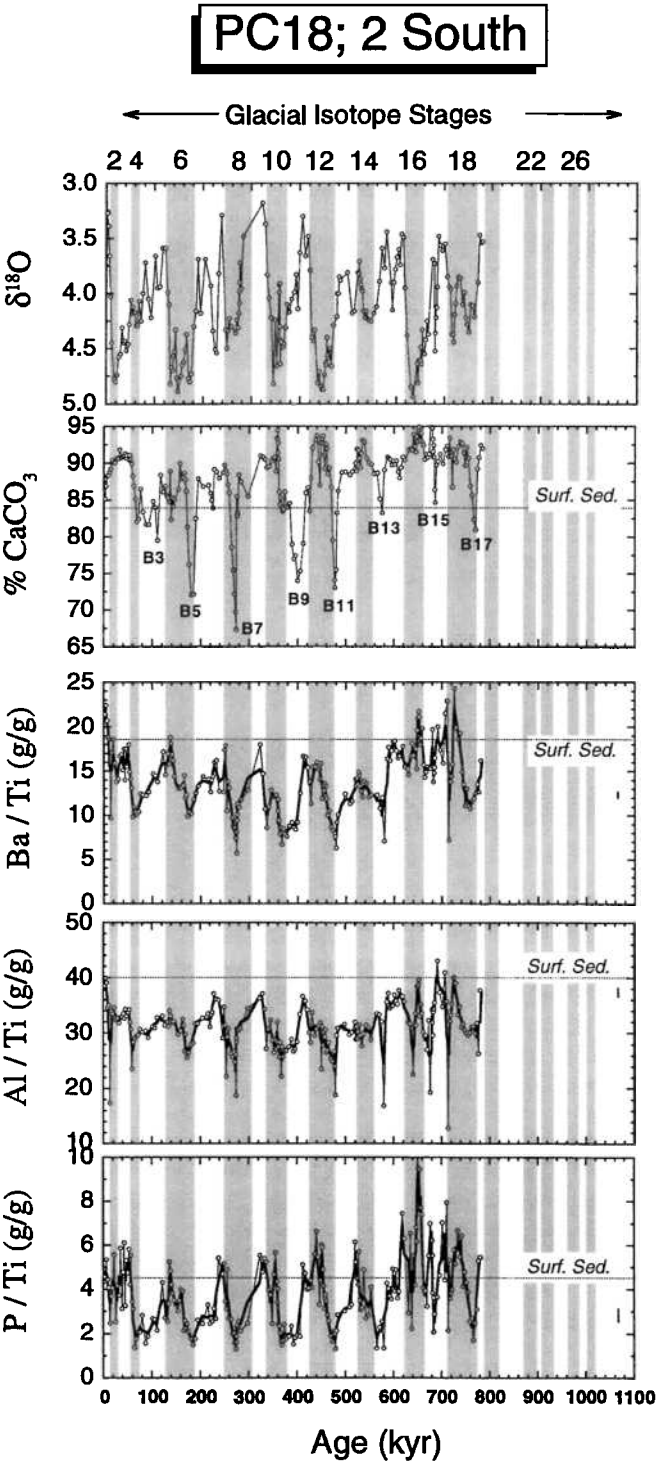

Figure 5. Age profiles of $\delta^{18}O$, percent $CaCO_3$ (wt %), and the chemical proxies (g/g) in core PC18, located at 2°S. For description of symbols and shaded regions, see Figure 4.

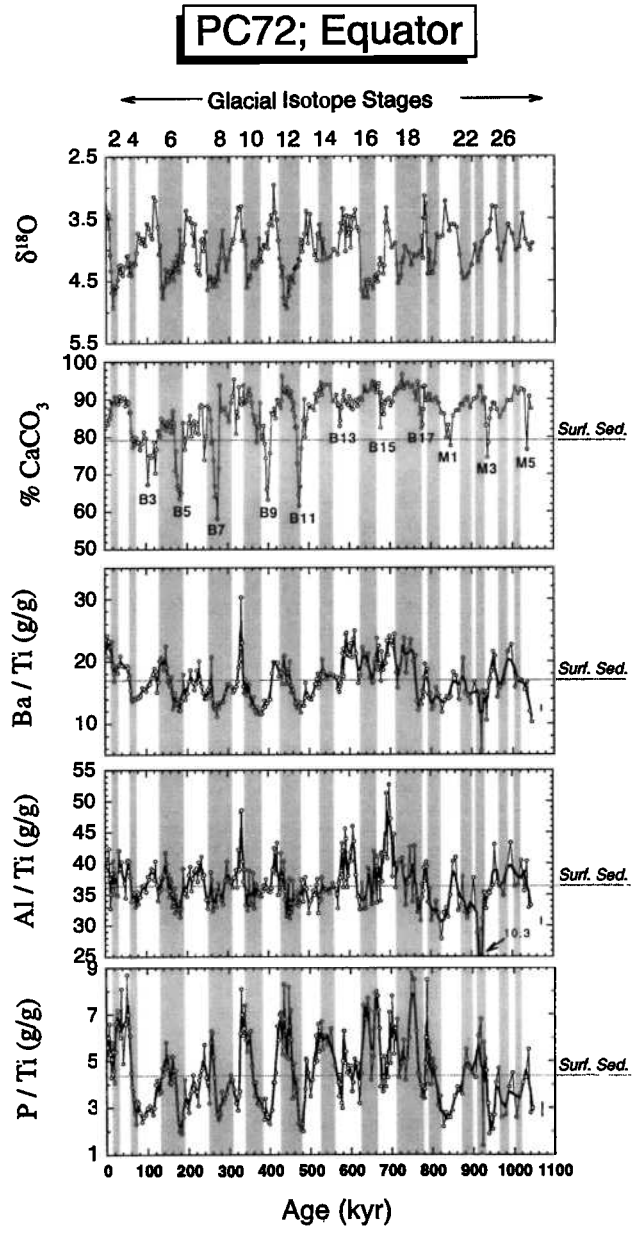

Figure 6. Age profiles of $\delta^{18}O$, percent $CaCO_3$ (wt %), and the chemical proxies (g/g) in core PC72, located at the equator. For description of symbols and shaded regions, see Figure 4.

marked broad increase in the average values of the paleoexport proxies, combined with a decrease in their dynamic range. This broad increase appears in all proxies at approximately the same time and is coincident with the center of the longer period percent $CaCO_3$ cycle and the decrease in the magnitude of the percent $CaCO_3$ minima through carbonate stages B11-B17. In PC32 (5°S) this is manifest as a well-defined two-peak maximum in carbonate stages B14 and B16 (at the terminations of glacial MIS 16 and MIS 18). At the equator it is characterized by a broad increase with less extreme minima in Ba/Ti and P/Ti as well as by two higher than usual maxima in Al/Ti.

6. The maxima in the proxies are more sharply peaked than the relatively broad ("flat") maxima in percent $CaCO_3$, whereas conversely the minima in the proxies are more broad than the narrow minima in percent $CaCO_3$. The proxies are generally lower compared to their values in surface sediment at the same latitude, with the exception of at the equator (PC72), where values are approximately the same. Values of the proxies at all latitudes are always greater than in PAAS (Ba/Ti = 0.11, Al/Ti = 16.7, and P/Ti = 0.12 [*Taylor and McLennan*, 1985]) with the exception of Al/Ti in PC32 (5°S), which we attribute to the detrital nature of the Al and Ti sourced from the OIBs from the Marquesas Islands [*Desonie et al.*, 1993].

7. The behavior of the proxies in PC114 (4°N) is very similar to that in PC32 (5°S), although PC32 displays a remarkably long period from ~500 to 200 kyr with few significant increases or decreases in any proxy. These two higher-latitude cores record one end-member of stratigraphic variation in the proxies, with PC72 (equator) being another end-member. Cores PC18 (2°S) and PC83 (2°N) are mixes of these two endmembers.

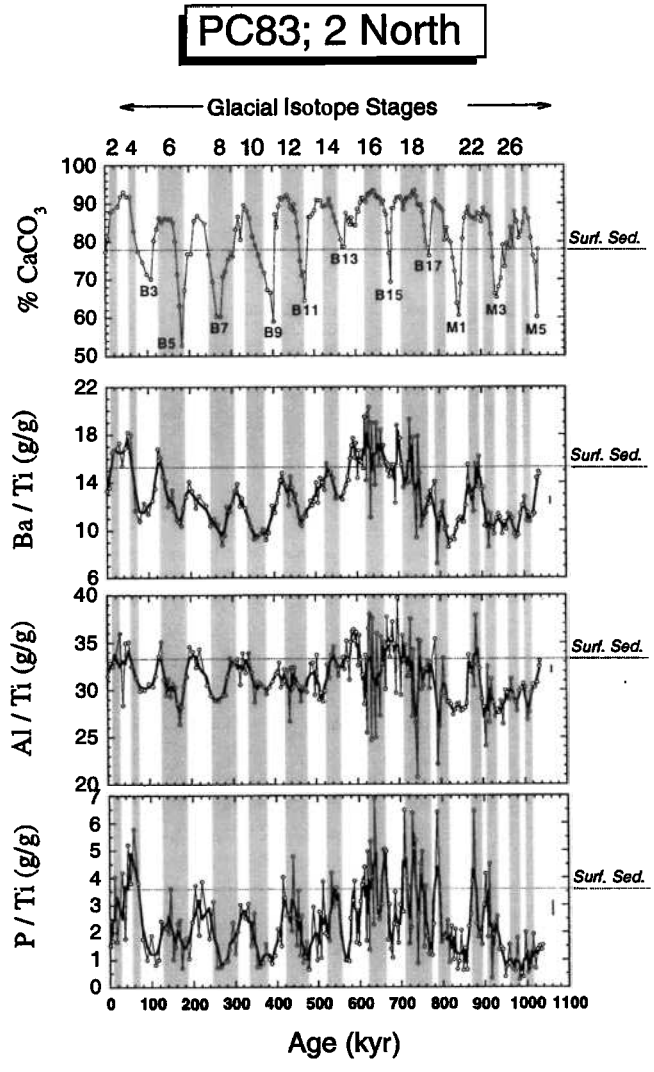

Figure 7. Age profiles of percent $CaCO_3$ (wt %) and the chemical proxies (g/g) in core PC83, located at 2°N. For description of symbols and shaded regions, see Figure 4.

8. The absolute changes in the proxies appear greatest at 2°S and the equator, while the very large relative changes at higher latitudes (e.g., the nearly factor of 2 increase in Ba/Ti and P/Ti from 0-500 kyr in core PC114 (4°N) (Figure 8) are barely recognizable in Figure 9.

5.3. Meridional Averages of Glacial-Interglacial Time Slices

Considering these records in the context of the time slice averages of Table 2 compares the average carbonate maxima proxy data to the proxy data found in the carbonate minima (Figure 10). Qualitatively, the proxies indicate greater export production during carbonate maxima, with the records from the lowest latitudes showing the greatest changes in absolute value. However, in many cases the higher latitudes show the greatest relative change. For Ba/Ti and Al/Ti through the 560-800 kyr interval it appears that at all latitudes there is minimal or no change in paleo-export, although that time frame itself is high in export. The P/Ti record shows the greatest variability, even through the 560-800 kyr interval.

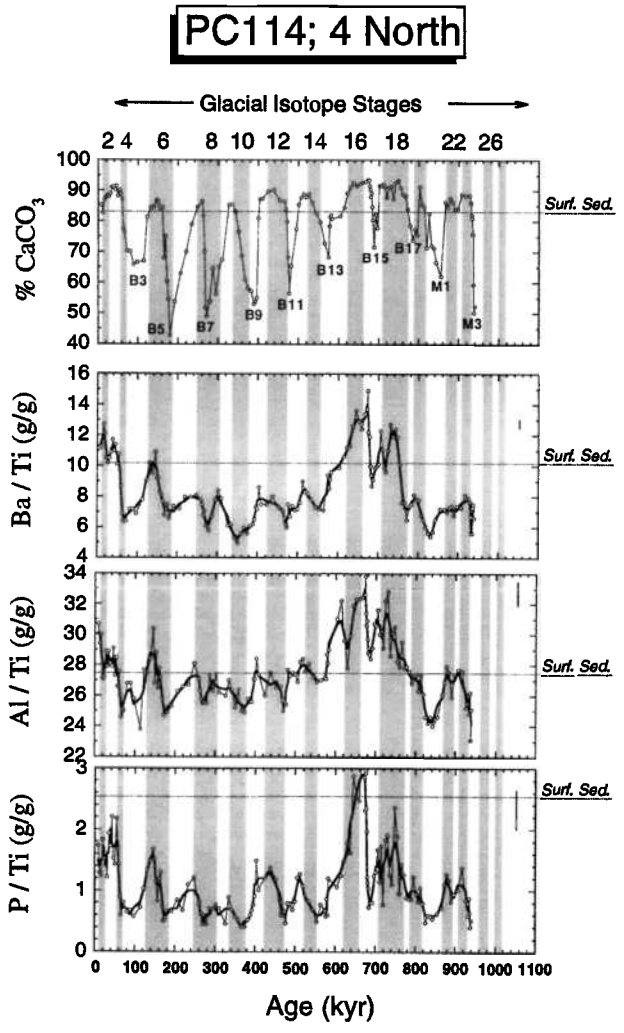

Figure 8. Age profiles of percent $CaCO_3$ (wt %) and the chemical proxies (g/g) in core PC114, located at 4°N. For description of symbols and shaded regions, see Figure 4.

The data set allows comparison of meridional gradients through time. Accordingly, we are able plot each core's time slice average (Table 2) of Ba/Ti (Figure 11), Al/Ti (Figure 12), and P/Ti (Figure 13) back to carbonate stage M5. Although the oldest carbonate stages (M1 to M5) are not completely recovered in all cores, relevant information can still be gathered. Within each figure all ordinate axes are plotted to a common scale in order to facilitate comparison. Several features appear:

1. All three proxies consistently indicate that export production has always been greatest at the equator.

2. The meridional pattern is always an inverted "V" pattern, similar to that observed along the surface transect and unlike the presence/absence meridional gradient of percent $CaCO_3$ (Figure 2).

3. The B2 carbonate maximum (centered at 30 kyr) (Table 2) appears to be similar to the average from the surface sediment.

4. Considering Ba/Ti and Al/Ti, from the B3 carbonate minimum to the B12 carbonate maximum (for Al/Ti and except for B9/B10) or the B14 maximum (for Ba/Ti), export production during carbonate maxima appears to be greater at essentially all latitudes, whereas from the older stages from B13 (for Al/Ti) or B15 (for Ba/Ti) to the oldest material recovered, there appears to be little or no contrast in export production.

5. The P/Ti record yields the greatest contrast in P/Ti between carbonate maxima and carbonate minima, with the carbonate minima recording extremely low relative P/Ti.

6. Much of the variability in the proxies appears to have the effect of geographically widening and narrowing the latitudinal width of export production, in that the greatest relative changes in the magnitude of a given proxy appear to occur at 2°S and 2°N, while the equator either increases modestly or not at all and the highest latitudes are relatively invariant. This phenomenon is most pronounced for Ba/Ti when comparing the changes between carbonate stages B12 and B11, B14 and B13, and M0 and B17 (Figure 11), while for Al/Ti it is present between B5 and B6, B12 and B11, B14 and B13, B16 and B15, and M0 and B17 (Figure 12). While we take care to not overinterpret this phenomena, it appears to be widespread. *Weber and Pisias* (1999), in an insightful study of ocean history in the Peru Basin, also documented glacial expansion and interglacial contraction of the equatorial upwelling system during many of these time periods.

6. Quantification of Variations in Export Production

The above discussions have been qualitative. The five-core data set allows us to quantify, however, the total export production across the latitudinal range 5°S-4°N over the past ~1 Myr, with respect to the modern values recorded by the surface sediment. This is achieved through use of the individual panels in Figures 11, 12, and 13 and integrating the "area under the curve" (Figure 14). This regional calculation is more quantitative than any comparison based on proxy changes in a single core. We have calculated the area under the

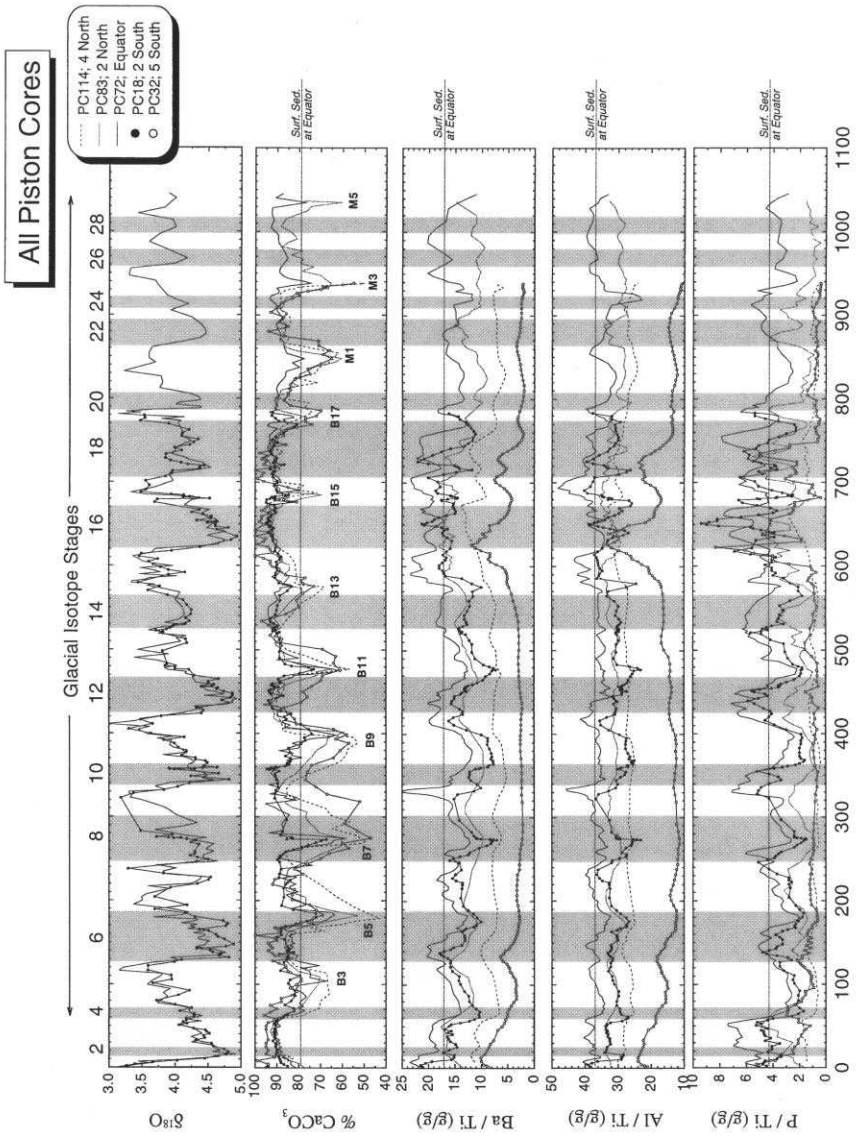

Figure 9. Summary of Figures 4-8, with all data plotted to common scales. Representative analytical precision is given in the text and in Figures 4-8. For description of symbols and shaded regions, see Figure 4.

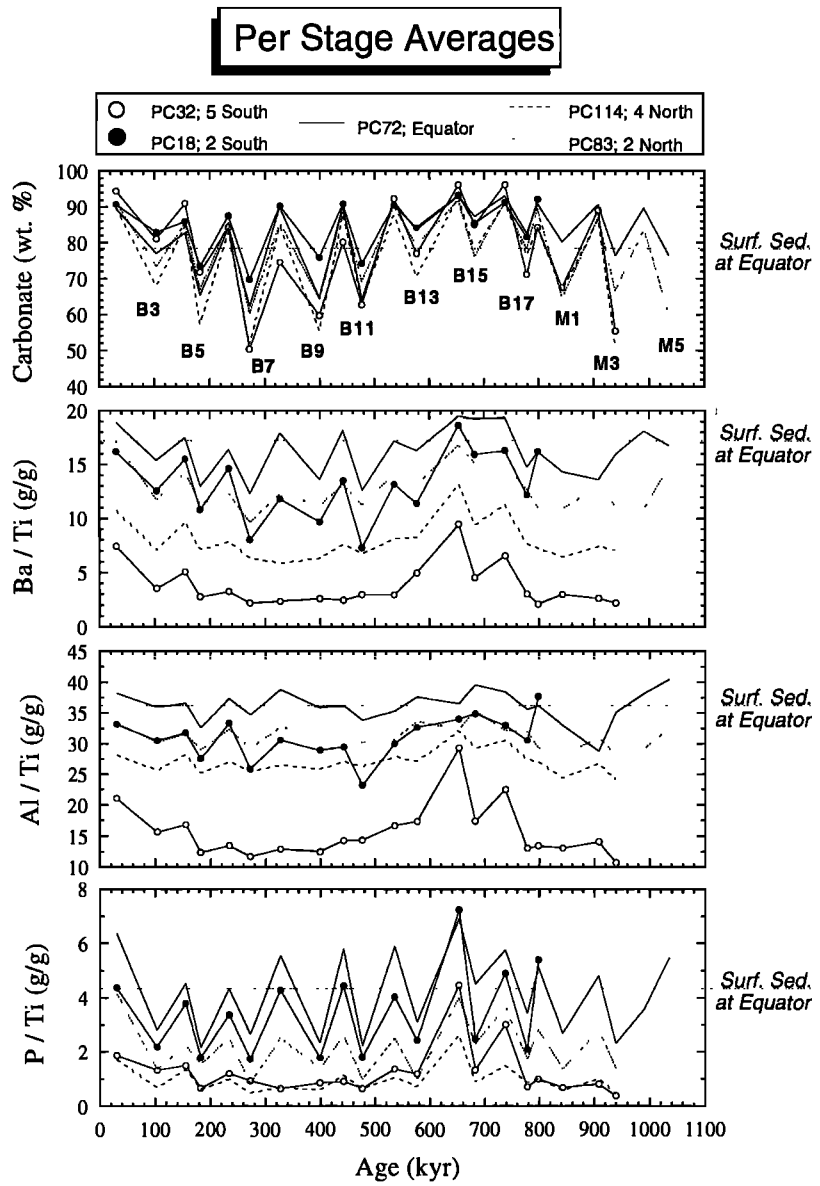

Figure 10. Age profiles of time slice average values of percent $CaCO_3$ (wt %) and the three chemical proxies (g/g) in all cores plotted at a common scale. Time slice averages are calculated using time intervals listed in Table 2. Representative analytical precision is given in the text and in Figures 4-8. Carbonate minima stages from *Farrell and Prell* [1989] and *Snoeckx and Rea* [1994, and references therein] In each panel the value of the given parameter at the equator (Figure 2) is shown by the dashed line.

curve only through the latitudinal range explicitly sampled by these cores (i.e., 5°S-4°N) (Figure 14). For baseline values we have extended (vertically downward on Figure 14) the values at the end of our piston core transect to those minimum values at the higher latitudes of the surface sediment transect from Figure 2. This is based on the assumption that the higher latitude sites have the lowest baseline export flux, which is reasonable given their considerable distance from the equator and the extremely low values of the export proxies at those latitudes. This assumption is further supported by a plethora of studies of the modern equatorial ocean [*Murray*, 1995, 1996; *Murray et al.*, 1997]. To summarize, then, the results of this quantification must strictly be interpreted only as assessing changes in export production between 5°S and 4°N.

Results (Table 4) are expressed as a ratio of a given glacial carbonate stage to the next youngest interglacial carbonate stage (e.g., the sum of the two shaded areas in Figure 14 divided by the smaller darker shaded area). As was visually evident from examination of the individual cores (Figs. 4-8) and the time slices along the meridional transect (Figs. 11-13), there are two main temporal domains, one younger than carbonate stage B13/B14 and the other older. In the younger domain, export production is, on average, 15% (using Al/Ti) or 31% (using Ba/Ti) greater during carbonate maxima than during carbonate minima, while in the older section export production appears to be, on average, 5% (using Ba/Ti) or 1% (using Al/Ti) greater during carbonate maxima. Given the intrinsic limitations of the database and proxies, we consider

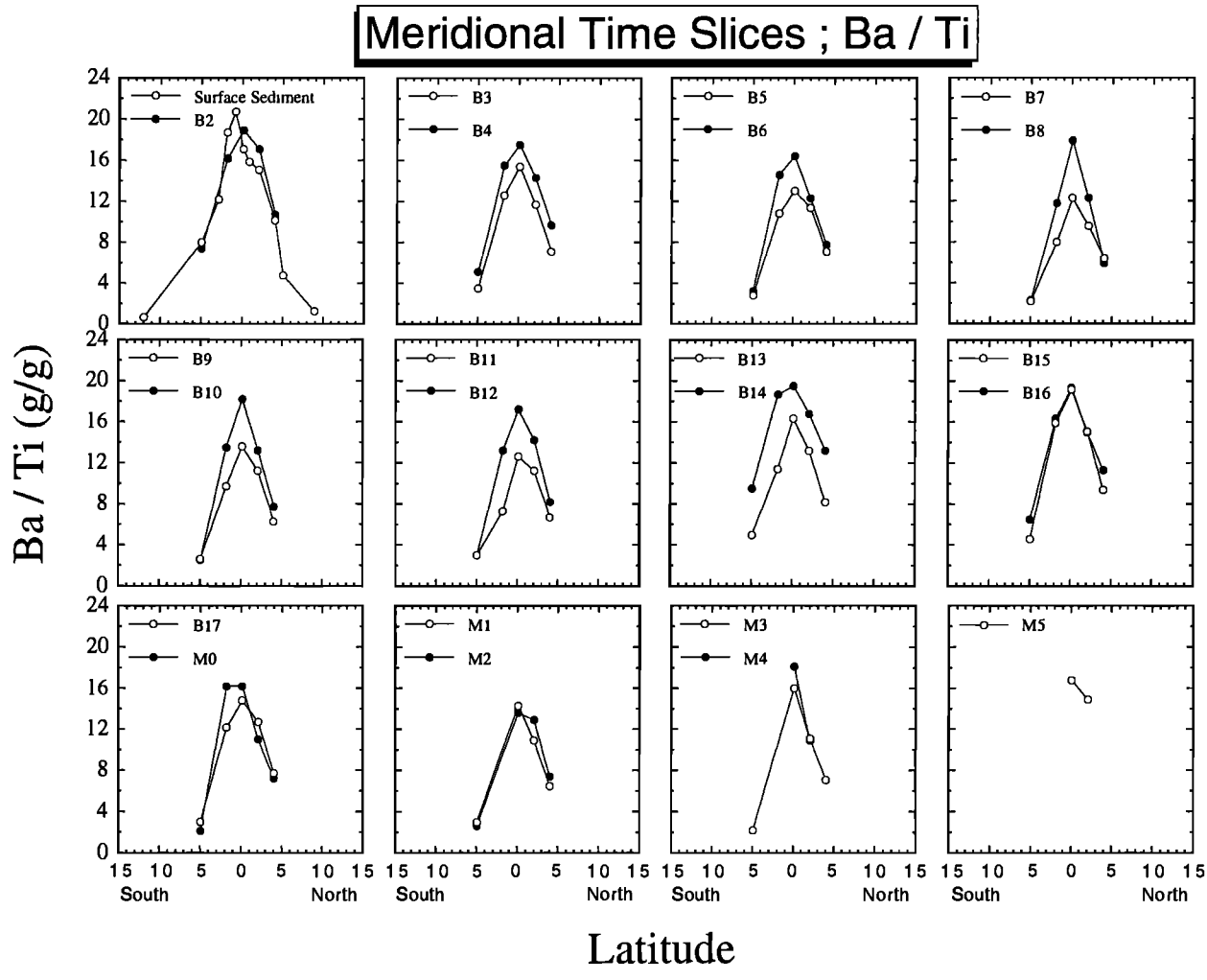

Figure 11. Meridional time slice averages of Ba/Ti (g/g), calculated using time intervals listed in Table 2. Representative analytical precision is given in the text and in Figures 4-8 Surface sediment (top left panel) is from Figure 2.

these values of 5% and 1% to be effectively "zero." Additionally, export production during stage B2 appears to have been the same as is recorded in the modern surface transect.

Values based on P/Ti are significantly greater than those based on Ba/Ti or Al/Ti. Although the shape of the meridional time slices of P/Ti and the relative behavior of P/Ti (i.e., higher values during carbonate maxima) are the same as that provided by Ba/Ti and Al/Ti, the absolute magnitude of the areally integrated P/Ti response (a two-fold to four-fold increase) appears unrealistically large. We believe these values to be compromised by diagenetic regeneration of P. The alternative (that the P data set is relatively primary) would require that this large increase not be recorded in the more stable Ba and Al. While this is not impossible, it is improbable, considering the reactivity of elemental P in bulk sediment compared to the more refractory nature of both Ba and Al. The very low values of P/Ti during interglacial periods supports this interpretation; during these times of slower sedimentation the reactive P is more likely to be efficiently remobilized. Additionally, because $CaCO_3$ provides a strong template for the formation of authigenic carbonate fluorapatite, which is a sink for diagenetically released P [*Filippelli and Delaney*, 1996], the lower carbonate interglacials will have a lower retention of the primary P signal. These interpretations are also supported by the time series analysis of the variability of P/Ti and percent $CaCO_3$ in core PC72, as will be discussed below.

Last, although the Ba/Ti-based results give consistently greater increases than the Al/Ti-based results, both ratios yield similar patterns of change through time (Figure 15a). Both ratios also indicate that over the past 600 kyr export production during both glacial and interglacial periods has been lower than it has been over the past 0.3-1.0 kyr recorded by the surface sediment transect (Figure 15b). Most of this difference is due to the changes at the higher latitudes; whereas at the equator only the carbonate minima record lower export through time, at the progressively higher latitudes both carbonate maxima and minima appear to have experienced lower export. This is most pronounced in the Southern Hemisphere. Therefore, we conclude that only through the 560-800 kyr period of time, in which occurred a broad increase in export production, has export in the equatorial Pacific approached or exceeded that of the Holocene (Figure 15b).

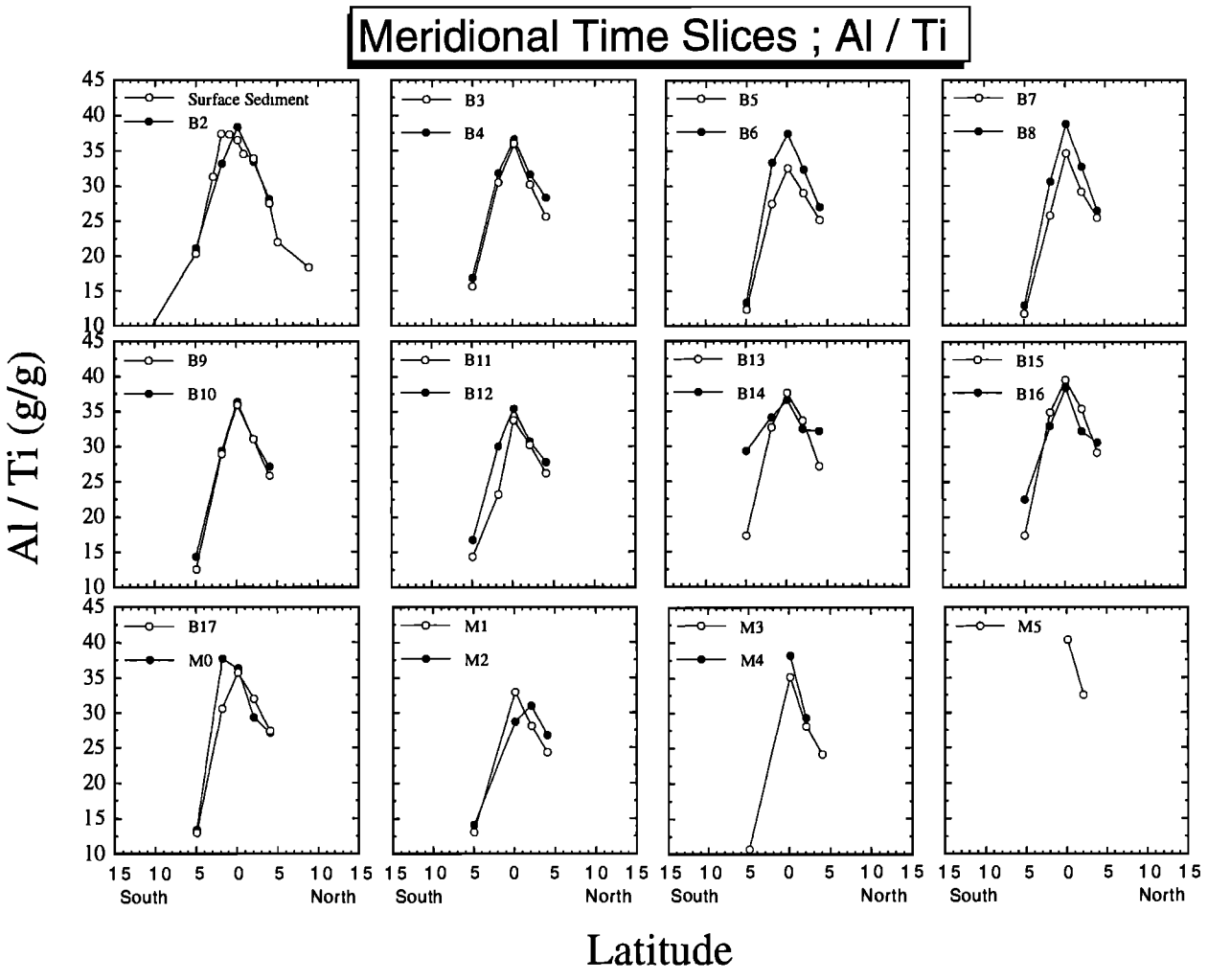

Figure 12. Meridional time slice averages of Al/Ti (g/g), calculated using time intervals listed in Table 2. Representative analytical precision is given in the text and in Figures 4-8. Surface sediment (top left panel) is from Figure 2.

Recalling that diagenetic modification of the primary signal is likely to a certain degree, we nonetheless feel this overall trend is not a secondary overprint. Analogous to the fact that each proxy is responding to a different aspect of the water column biogeochemical cycling, each will also respond differently to diagenesis (e.g., Ba being affected by redox degradation of oxides, Al_{excess} potentially being affected by dissolution of opal, and P being affected by the degradation of C_{org}). That the proxies all provide similar records, and that these records also show increases at greater subseafloor depths rather than a consistent decrease with age to the bottom of each core, are most consistent with the collected patterns (particularly of Ba/Ti and Al/Ti) recording a dominantly primary signal.

7. Export Production and Dissolution Over the Past 1 Myr

7.1. Magnitude of Increases in Export Production

The data derived from these five cores indicate that over the past 560 kyr export production throughout the equatorial upwelling region has been greater during the carbonate-defined glacial periods than during interglacials. While the records clearly show that not all periods behave identically, the pattern of greater export during carbonate maxima is robust. The areal integration indicates that from 5°S to 4°N during glacial time periods of the past 560 kyr, export production was, on average, 15-30% greater than during interglacial climatic conditions (Figure 15a and Table 4). These values are consistent with interpretations based on $\delta^{15}N$ records in the region [*Farrell et al.*, 1995]. Both the Ba/Ti and Al/Ti proxies indicate that maximum glacial increases can be up to 50% greater. These figures are substantially less than the factor of 2 increase postulated by *Paytan et al.* [1996] in a study of barite accumulation in JGOFS cores. Even though *Paytan et al.* [1996] studied only the past several 100 kyr, our results from the same time period as their data set yield values in the range of 20-30% greater. Even if one were to consider the P/Ti data, which we have questioned because concerns about diagenetic modifications, our conclusions remain the same. Thus, while our results confirm the pattern of greater export during glacial periods of *Paytan et al.* [1996], our quantification suggests a less extreme increase and is more consistent with the interpretations of *Farrell et al.* [1995].

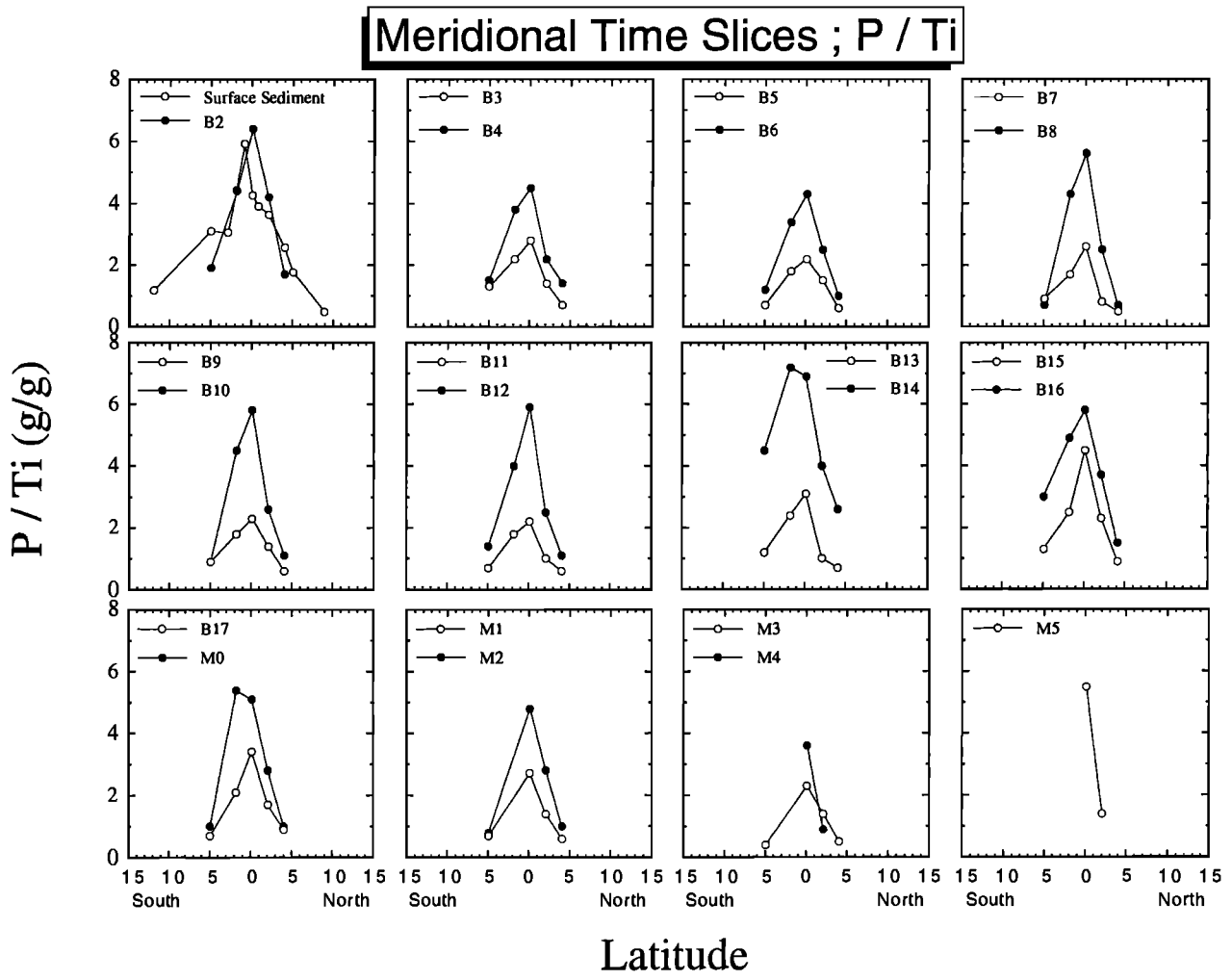

Figure 13. Meridional time slice averages of P/Ti (g/g), calculated using time intervals listed in Table 2. Representative analytical precision is given in the text and in Figures 4-8. Surface sediment (top left panel) from Figure 2.

7.2. Mid-Pleistocene Climate Transition

The period from 800 to 560 kyr is markedly different from the younger record across the entire meridional transect. For example, at 5°S and 4°N, although the absolute magnitude of export production is relatively low compared to the lower latitudes (Figure 9), export doubled or tripled over the background values at the same latitude (Figures 4 and 8). The lower latitude cores also record a greatly increased frequency of variation. Considering the region on the whole, this requires an extremely large increase in export production from the previously low values (Figures 15b). The temporal center of this phenomenon coincides with the B14-B16 maximum in the long-period $CaCO_3$ cycle as well.

This interval broadly coincides with the Mid-Pleistocene climate Transition (MPT), in which oxygen isotopic records indicate a global shift from a 41 kyr cyclicity to the late Pleistocene 100 kyr cyclicity [*Raymo et al.*, 1997; *Mudelsee and Schulz*, 1997; *Mudelsee and Statteger*, 1997, and references therein]. As noted by *Raymo et al.* [1997], while the timing of the MPT is commonly ascribed to ~900 kyr, it is not until ~700 kyrs (MIS 17) that the 100 kyr cyclicity becomes dominant. Thus, there is temporal overlap between the MPT and the extreme increase in export production we observe, with the equatorial increase occurring during and shortly after the MPT. *Raymo et al.* [1997] documented that changes in the absolute $\delta^{13}C$ composition of the global ocean occurred in association with the MPT and hypothesized that the changes in $\delta^{13}C$ are responding to a "one-time addition" of depleted, terrestrially derived organic carbon into the ocean. On the basis of an unchanging Atlantic-Pacific $\delta^{13}C$ gradient, however, *Raymo et al.* [1997] also suggested there was no change in the mean ocean nutrient content during the isotopic shift, which implies that the large increase in export production in the equatorial Pacific Ocean during this period is not caused by the simple addition of nutrients to the global ocean. Thus, if the Pacific increase is indeed related to global MPT changes, it appears to require a strongly local response. Future studies will more specifically address the relative timing of these events and assess quantitatively whether the increase in export production we observe during and shortly after the MPT can realistically be linked to the changing ocean-atmosphere state through that time period.

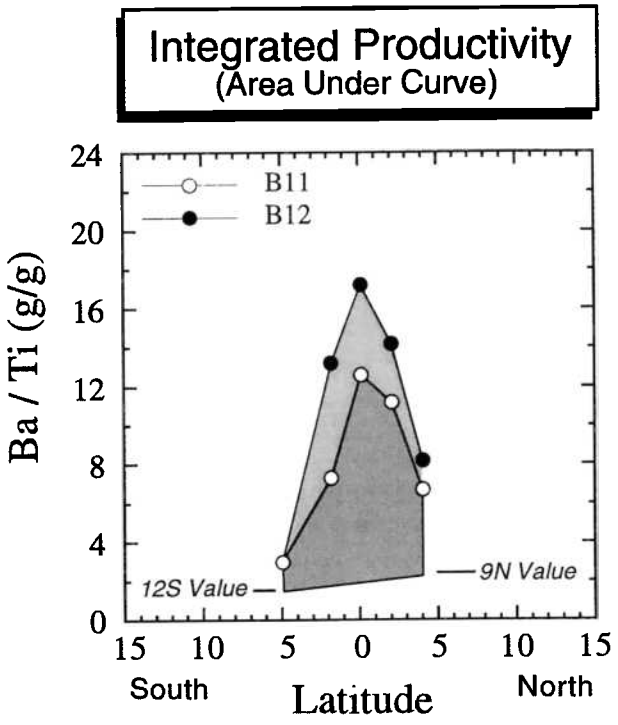

Figure 14. "Area under the curve" method of calculating meridionally integrated values of paleoexport production, using Ba/Ti in carbonate stages B11 and B12 (from Figure 11) as an example. 12°S and 9°N values are from Figure 2. Modified from *Murray et al.* [2000].

7.3. Increases in Export Production Occurring During Glacial Transitions

The time series analysis of core PC72 provides additional information regarding temporal variations in export production (Table 5 and Figure 16). In addition to analyzing the entire 0-1044 kyr record, we studied the 0-564 kyr and 564-1044 kyr portions in order to compare the two temporal domains. Owing to the intrinsic limitations of the chemical data set described above, we hesitate to interpret the time series beyond looking for broad common trends. For example, there are small leads and lags of the proxies between themselves (Table 5), which we attribute to the different proxy's response to a different aspect of the marine biogeochemical cycle as well as each having differing burial characteristics. Taken collectively, however, the cross-spectral analyses of the different variables is informative, particularly since the preceeding discussions of meridional and time slice averages by definition were limited to study of the 100 kyr cyclicity in percent $CaCO_3$.

Where coherent, the percent $CaCO_3$ and $\delta^{18}O$ records show the well-known lag of $CaCO_3$ with respect to $\delta^{18}O$ [*Farrell and Prell*, 1989; *Snoeckx and Rea*, 1994; and references therein]. The database records the strongest coherency in the 100 kyr band over the 0-564 kyr period, as well as throughout the entire 0-1044 kyr record, but this coherency diminishes or disappears when the older 564-1044 kyr portion is considered alone.

Considering first the relationships of the chemical proxies to $\delta^{18}O$, both Ba/Ti and Al/Ti tend to lag behind $\delta^{18}O$ in the 100 kyr band (as does P/Ti, but less so) and, for Ba/Ti, in the 41 kyr band. This lag indicates that the maxima in export production are associated with glacial transitions and not glacial maxima conditions. Moreover, there is no discernable difference in cross-spectral character of Al/Ti and $\delta^{18}O$ in the 100 kyr band between the 0-564 and the 564-1044 kyr portion of the records, yet there is a pronounced change between these time periods in the 41 kyr band. While there is no coherency between Al/Ti and $\delta^{18}O$ over the shorter time frame, the linkage during the older portion of the record is much stronger (coherency equals 0.79) which is in phase with interglacial time periods (phase angle within error of 180° of glacial times). This older sequence apparently dominates the spectral character of the long record, for the 0-1044 kyr analysis yields essentially the same result as that of 564-1044 kyr (Table 5). The P/Ti record also shows a strong interglacial tie to $\delta^{18}O$ in the 23 kyr band. Finally, it is clear that Ba/Ti and Al/Ti are most strongly tied to percent $CaCO_3$ in the 100 kyr band, with high coherency, and also show the characteristic lag toward the glacial transitions, although this is less extreme (lower phase angles) than is the case when comparing to $\delta^{18}O$. As above, the Al/Ti record is markedly different, with respect to percent $CaCO_3$, from 0 to 564 and 564 to 1044 kyr. The spectral relationship between P/Ti and percent $CaCO_3$ is discussed later.

7.4. Spatial Variability in Export Production

At all time periods, export production has been greater at the equator than at the higher latitudes in either hemisphere (Figures 11-13). The overall inverted V pattern has been maintained over the past 1 Myr, and has been continually different from the meridional presence/absence pattern of percent $CaCO_3$ (Figure 2). The pattern of export production at high latitudes is dominated by the increase during and after the MPT followed by a long period of relatively little change until the last 100-150 kyr (Figures 4, 8, and 9). The change through the MPT is not as dominant at the lower latitudes with respect to the entire time period because of the strength of the Milankovitch-scale cyclicity in export production at those locations.

Table 4. Changes in Export Production Between Carbonate Stages

Stage to Stage	Proxy		
	Ba-Based	Al-Based	P-Based
B2 to Holocene	0.99	0.98	0.98
B4-B3	1.23	1.09	2.07
B6-B5	1.28	1.24	2.04
B8-B7	1.38	1.35	3.57
B10-B9	1.30	1.02	3.08
B12-B11	1.45	1.24	3.17
B14-B13	1.52	1.14	4.39
B16-B15	1.05	0.98	1.98
M0-B17	1.07	1.09	2.11
M2-M1	1.02	0 96	1.83
Average ≤ B14-B13	1.31	1.15	2.76
Average > B14-B13	1.05	1.01	1.97

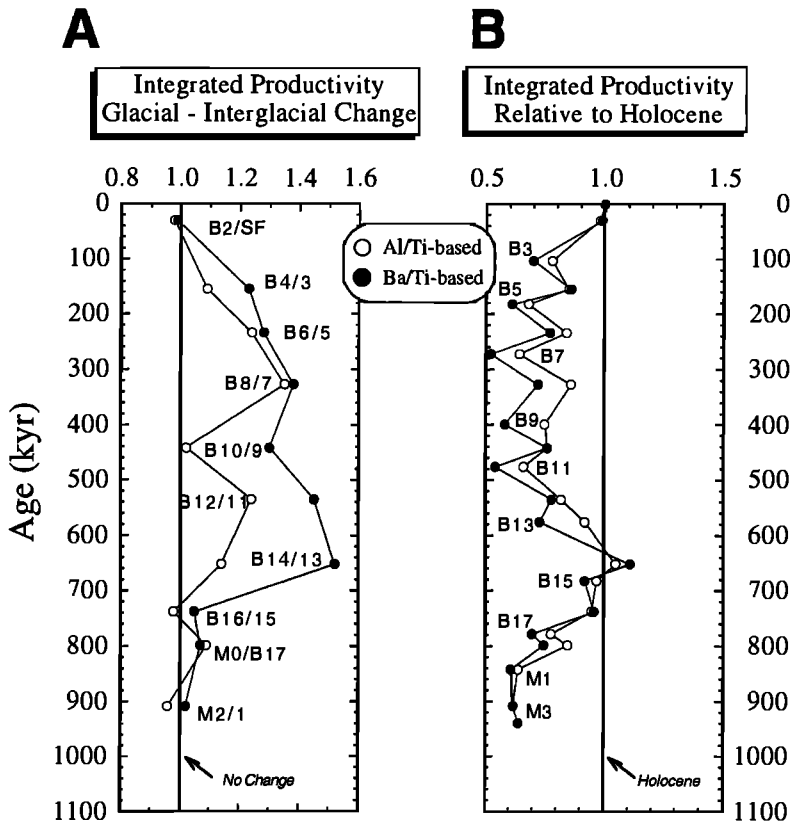

Figure 15. (a) Comparison of glacial to "next younger interglacial" stage of integrated area under the curve values of the productivity proxies, using both the Ba/Ti and Al/Ti based values. Data are plotted from Table 4. (b) Integrated values plotted as normalized to the value from the surface sediment. Thus, only carbonate stages B14-B16 experienced export production as high as the most recent average. In both panels, carbonate minima stages are from *Farrell and Prell* [1989] and *Snoeckx and Rea* [1994, and references therein].

When comparing glacial-interglacial variability in export production at any single location, it is not appropriate to use the areally integrated values derived above (e.g., Figure 14). Instead, we need to document that at any one location there is a relationship between the proxies and export production. In order to achieve this we return to the surface sediment transects (Figure 2) and exploit the apparent linear response of both Ba/Ti and Al/Ti to surface water productivity (Figure 17). Because of this linearity we can convert changes in these proxies to changes in export at one location. Averaging values of both Ba/Ti and Al/Ti from the carbonate minima and maxima from ~0 to 564 kyr as well as through the general 560-800 kyr increase (Figures 6 and 8), and applying the regressions from Figure 17, indicates that productivity at the equator (PC72) has increased during carbonate glacials relative to interglacials by 20-30% during the younger portion of the record and by 20-30% through the older portion. At 4N, these values are 10-15% and 10-20%, respectively. This confirms our previous observation that while there are large relative changes at higher latitudes, the greatest absolute change occurs nearest the equator.

7.5. Carbonate Dissolution: Temporal and Spatial Variability

These export production proxy records can be used to help explain not only the "productivity" contribution to these cycles but also the "dissolution" contribution. While there is little to no change in the absolute extent of paleoexport at the highest latitudes (e.g., Figure 9), it is precisely in these higher latitude cores that the greatest changes in percent $CaCO_3$ are found (Figures 4-8). Given that the overall absolute magnitudes of the export flux are uniformly low at these higher latitudes, however, it is unlikely that the small variations in absolute flux can be responsible for the extremely developed percent $CaCO_3$ maxima and minima. This suggests that dissolution and preservation mechanisms are a stronger control on the percent $CaCO_3$ record at the highest latitudes than at the lower latitudes. In the absence of dissolution, changes in export alone at these high latitudes would require an unrealistic amplification of that export signal. Thus, although export clearly shows strong glacial increases at the higher latitudes, it appears that dissolution is a very important control on the percent $CaCO_3$ cyclicity there.

This hypothesis can be tested in the future by considering the potential effects of variations in C_{org} burial, distribution of silica, and bottom water carbonate chemistry on the preservation capacity of the carbonate [e.g., *Emerson et al.*, 1980; *Emerson and Bender*, 1981; *Grundmanis and Murray*, 1982; *Emerson*, 1985; *Berelson et al.*, 1990a, 1990b, 1997; *Martin et al.*, 1991; *Jahnke et al.*, 1994; and references therein]. Studies of the relationships between carbonate dissolution indices [e.g., *Berger*, 1970, 1972, 1973, 1977; *Peterson and Prell*, 1985; *Wu and Berger*, 1989; *Wei et al.*,

Table 5. Results of Cross-Spectral Analysis, Core TT013-PC72 (Equator) [a]

Variable 1 versus Variable 2	Phase Difference ± Phase Error , Coherency , kiloyears		
	100 kyr	41 kyr	23 kyr
$\delta^{18}O$ versus Site 677			
0-564 kyr	4 ± 7 ; 0 95	12 ± 13 , 0.87	- 12 ± 14 ; 0.85
564-1044 kyr	3 ± 8 , 0 96	12 ± 90 ; 1.00	- 36 ± 32 ; 0.58
0-1044 kyr	3 ± 5 , 0.96	12 ± 6 ; 0.94	- 21 ± 16 , 0 72
Percent $CaCO_3$ versus $\delta^{18}O$			
0-564 kyr	- 53 ± 19 ; 0.76 ; 15	- 113 ± 18 ; 0.78 ; 13	
564-1044 kyr	19 ± 20 ; 0 75		
0-1044 kyr	- 38 ± 18 ; 0.67 ; 11		
Ba/Ti vs $\delta^{18}O$			
0-564 kyr	- 88 ± 12 ; 0 88 ; 24	- 123 ± 26 ; 0.64 ; 14	
564-1044 kyr			
0-1044 kyr	- 94 ± 13 ; 0.78 , 26	- 122 ± 20 ; 0.64 ; 14	
Al/Ti versus $\delta^{18}O$			
0-564 kyr	- 110 ± 17 ; 0.79 ; 31		
564-1044 kyr	- 140 ± 26 ; 0.67 ; 39	195 ± 19 ; 0 79 ; 22	
0-1044 kyr	- 126 ± 17 ; 0.69 ; 35	194 ± 23 , 0.58 ; 22	
P/Ti versus $\delta^{18}O$			
0-564 kyr	- 53 ± 11 , 0.89 ; 15	- 92 ± 18 , 0.77 , 10	- 192 ± 15 ; 0 83 ; 12
564-1044 kyr	13 ± 18 ; 0 80	- 65 ± 17 , 0.82 ; 7	
0-1044 kyr	- 40 ± 13 ; 0 80 ; 11	- 76 ± 14 ; 0.76 ; 9	- 196 ± 13 ; 0.79 , 13
Ba/Ti vs Percent $CaCO_3$			
0-564 kyr	- 27 ± 11 ; 0.90 ; 8		
564-1044 kyr			
0-1044 kyr	- 40 ± 14 ; 0.77 ; 11		- 31 ± 39 ; 0 55
Al/Ti versus Percent $CaCO_3$			
0-564 kyr	- 43 ± 16 , 0.82 ; 12		
564-1044 kyr	- 136 ± 20 ; 0 77 , 38	- 151 ± 24 ; 0.71 ; 17	
0-1044 kyr	- 73 ± 28 , 0.49 ; 20		
P/Ti versus Percent $CaCO_3$			
0-564 kyr	0 ± 11 ; 0 90		
564-1044 kyr	2 ± 17 , 0 81		
0-1044 kyr	0 ± 9 ; 0.88		
Ba/Ti versus Al/Ti			
0-564 kyr	17 ± 11 ; 0 90 ; 5		
564-1044 kyr			
0-1044 kyr	18 ± 14 , 0 77 , 5		
Ba/Ti versus P/Ti			
0-564 kyr	- 31 ± 9 ; 0 93 ; 9	- 33 ± 17 , 0.80 , 4	
564-1044 kyr			
0-1044 kyr	- 45 ± 13 , 0.79 ; 13	- 37 ± 14 ; 0 77 ; 4	
Al/Ti versus P/Ti			
0-564 kyr	-53 ± 13 ; 0.87 ; 15		
564-1044 kyr			
0-1044 kyr	- 82 ± 29 ; 0.48 , 23	- 91 ± 27 ; 0 50 ; 10	

[a] Positive phase angles indicate that the first variable leads the second The test statistic for nonzero coherency at the 80% confidence level equals 0.57, 0.62, and 0.42, respectively, for the time intervals of 0-564 kyr (189 samples), 564-1044 kyr (161 samples), and 0-1044 kyr (349 samples). No phase angle is given if records are not coherent at the 80% confidence level or if one variable shows no significant change in variance within the period of interest. Interpolation and cross-spectral analyses performed at Δt = 3 kyr for given time interval (see text for selection of intervals) Bandwidth is 0.009 with 50 lags in each case.

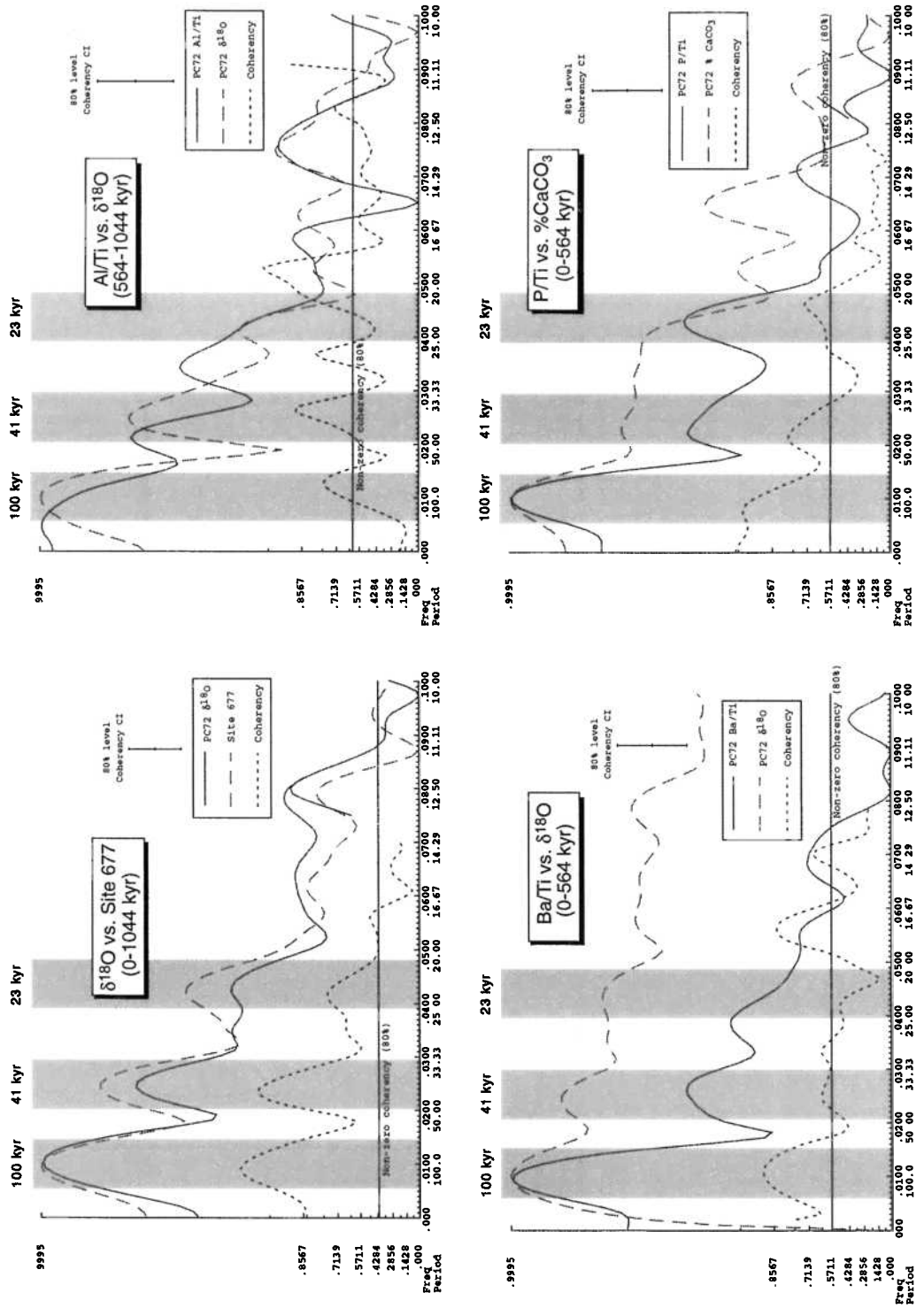

Figure 16. Cross-spectral diagrams of representative variables over several different time periods in core PC72. See Table 5 for additional cross-spectral results. Bandwidth is equal to shaded region of each period.

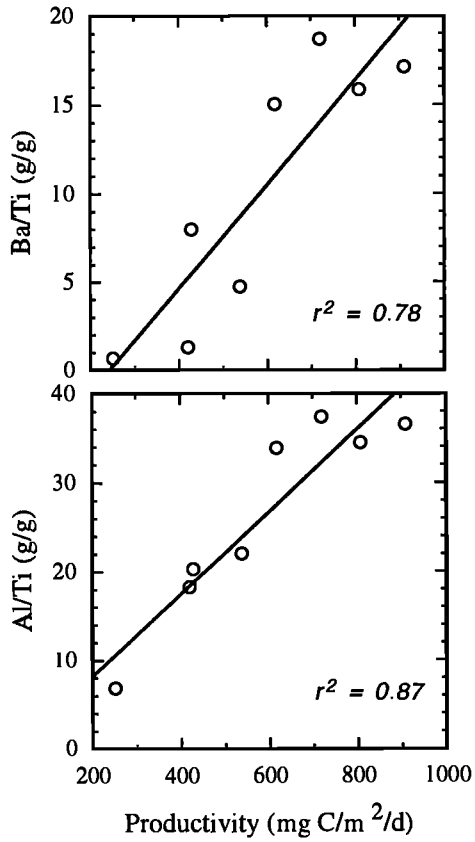

Figure 17. Linear relationships between Ba/Ti and Al/Ti in the 0-1 cm surface sediment and productivity of the uppermost surface waters (from Figure 2). Equations of lines are Ba/Ti = (0.030 x productivity) - 7, with an r^2 of 0.78, and Al/Ti = (0.046 x productivity) - 1, with an r^2 of 0.87.

1994; *LaMontagne et al.*, 1996], percent $CaCO_3$, and the chemical proxies of export production are also likely to yield insights into the relative timing of variations in dissolution intensity. For example, *LaMontagne et al.* [1996] documented in core WEC8803B-GC51 (1.3°N, 135°W) a broad 100 kyr cyclicity in dissolution intensity, confirming the general results of *Farrell and Prell* [1989, and references therein]. However, *LaMontagne et al.* [1996] further observed that the percent $CaCO_3$ record is not exactly coincident with variations in indices of foraminiferal dissolution, suggesting that carbonate deposition, dissolution intensity, and paleo-export may be decoupled.

The time series analysis of core PC72 also provides information relevant to carbonate dissolution (Table 5 and Figure 16). The patterns of P/Ti and percent $CaCO_3$ are closely related in the 100 kyr band (Table 5), possessing some of the strongest coherencies of the entire database. As mentioned above, for independent reasons we interpret the P/Ti record to be influenced by diagenetic remobilization, perhaps more extensively so during interglacials. That P/Ti and percent $CaCO_3$ are strongly in phase in the 100 kyr band is consistent with both these records having an important component of dissolution being responsible for their paired variability. Because P/Ti and percent $CaCO_3$ display such similar records over the longer period, the cross-spectral relationships of Ba/Ti and Al/Ti to P/Ti and to percent $CaCO_3$ are also similar (Table 5).

Finally, at all latitudes the proxy records are characterized by maxima that are sharper than the flat plateaus of the percent $CaCO_3$ maxima as well as by minima that, conversely, are more broad than the deeply incised percent $CaCO_3$ minima. This phenomenon is consistent with dissolution increasing the degree of the primary low value of percent $CaCO_3$ that results from the overall low export production during interglacials (thus resulting in the more narrow and sharp percent $CaCO_3$ minima). Thus, the periods of time with low export are longer in duration than the sharp minima in percent $CaCO_3$, while the periods of time with high export are shorter in duration than the broad plateaus of maximum $CaCO_3$. The significance of this pattern will be better assessed by future studies of the accumulation rates of the biogenic components in these cores.

8. Summary: Dynamic Changes in Export Production and Dissolution

Our collected data set is best explained by a combination of the two end-member processes (changes in export production and changes in dissolution intensity) simultaneously operating, with each process being more important at various locations in time and space. We have shown that changes in export production have occurred at all latitudes along the 140°W meridional transect and that glacial climatic states are characterized by greater export production, particularly over the past 560 kyr. Maxima in export occur during glacial transitions and are not directly coincident with glacial maxima. Glacial increases over this time period indicate a 15-30% increase in export, areally integrated across the 5°S to 4°N transect, with the equatorial system often meridionally expanding during glacials. Values through the past 560 kyr indicate that export production was lower than values in the Holocene, even during glacial periods. The biogeochemical processes in the central equatorial Pacific Ocean, however, were significantly different during the early Brunhes and MPT, with greatly increased export at the higher latitudes and minimal or zero glacial-to-interglacial contrast in export production throughout the region.

Because the absolute magnitude of glacial-interglacial variations in export production is latitudinally dependent, with higher latitudes being characterized by large relative changes but minimal absolute changes, it is unlikely that the climatically linked changes in export are dominantly responsible for the extremely developed minima in percent $CaCO_3$ at 5°S and 4°N. At these higher latitudes, carbonate dissolution appears to be more important than changes in export.

Acknowledgments. We thank J. Farrell, G Filippelli, and C. Ravelo for a great set of comments that improved the manuscript. Dave Murray (Brown University) has provided invaluable assistance throughout all aspects of this project, and we thank him for his generosity of time and effort Shore-based core curation, chemical analyses, and interpretation were supported by NSF grants OCE-9102410, OCE-9301097, OCE-9711464. This is U.S. JGOFS contribution number 558.

References

Adelseck, C.G., Jr, and T.F Anderson, The late Pleistocene record of productivity fluctuations in the eastern equatorial Pacific Ocean, *Geology, 6*, 388-391, 1978

Archer, D., Equatorial Pacific calcite preservation cycles: Production or dissolution?, *Paleoceanography, 6*, 561-571, 1991a

Archer, D, Modeling the calcite lysocline, *J. Geophys Res, 96*, 17,037-17,050, 1991b.

Arrhenius, G.O.S, Sediment cores from the east Pacific, in *Report of the Swedish Deep Sea Expedition, 1947-1948*, vol. 5, pp. 1-228, 1952

Arrhenius, G, Rate of production, dissolution and accumulation of biogenic solids in the ocean, *Palaeogeogr., Palaeoclimatol, Palaeoecol., 67*, 119-146, 1988

Banakar, V K., G Parthiban, J N. Pattan, and P Jauhari, Chemistry of surface sediment along a north-south transect across the equator in the central Indian Basin: an assessment of biogenic and detrital influences on elemental burial on the seafloor, *Chem. Geol, 147*, 217-232, 1998.

Berelson, W M., et al., Biogenic budgets of particle rain, benthic remineralization and sediment accumulation in the equatorial Pacific, *Deep Sea Res, 44*, 2251-2282, 1997.

Berelson, W M., D.E. Hammond, and G.A. Cutter, In situ measurements of calcium carbonate dissolution rates in deep-sea sediments, *Geochim Cosmochim. Acta, 54*, 3013-3020, 1990a

Berelson, W M, D E. Hammond, D O'Neill, X.-M. Xu, C Chin, and J. Zukin, Benthic fluxes and pore water studies from sediments of the central equatorial north Pacific: Nutrient diagenesis, *Geochim Cosmochim. Acta, 54*, 3001-3012, 1990b

Berger, W H., Biogenous deep-sea sediments fractionation by deep-sea circulation, *Geol Soc. Am Bull., 81*, 1385-1402, 1970.

Berger, W.H, Deep sea carbonates. Dissolution facies and age-depth constancy, *Nature, 236*, 392-395, 1972.

Berger, W.H., Deep-sea carbonates: Pleistocene dissolution cycles, *Journal of Foraminiferal Research, 3*, 187-195, 1973.

Berger, W.H, Deep-sea carbonate and the deglaciation preservation spike in pteropods and foraminifera, *Nature, 269*, 301-304, 1977.

Berger, W H., and J C Herguera, Reading the sedimentary record of the ocean's productivity, in *Primary Productivity and Biogeochemical Cycles in the Sea*, edited by P.G. Falkowski and A D Woodhead, pp. 455-486, Plenum, New York, 1992

Bishop, J.K.B, The barite-opal-organic carbon association in oceanic particulate matter, *Nature, 332*, 341-343, 1988.

Chuey, J M., D.K. Rea, and N.G. Pisias, Late Pleistocene paleoclimatology of the central equatorial Pacific: A quantitative record of eolian and carbonate deposition, *Quat. Res, 28*, 323-339, 1987.

Dehairs, F, R. Chesselet, and J. Jedwab, Discrete suspended particles of barite and the barium cycle in the open ocean, *Earth Planet Sci Lett, 49*, 528-550, 1980

Dehairs, F., C.E Lambert, R. Chesselet, and N. Risler, The biological cycle of marine suspended barite and the barium cycle in the western Mediterranean Sea, *Biogeochemistry, 4*, 119-139, 1987.

Dehairs, F., L Goeyens, N Stroobants, P. Bernard, C. Goyet, A. Poisson, and R Chesselet, On suspended barite and the oxygen minimum in the Southern Ocean, *Global Biogeochem. Cycles, 4*, 85-102, 1990.

Dehairs, F., W Baeyens, and L Goeyens, Accumulation of suspended barite at mesopelagic depths and export production in the southern ocean, *Science, 258*, 1332-1335, 1992.

Delaney, M.L, Phosphorous accumulation in marine sediments and the oceanic phosphorous cycle, *Global Biogeochem. Cycles, 12*, 563-572, 1998

Desonie, D L., R.A Duncan, and J.H. Natland, Temporal and geochemical variability of volcanic products of the Marquesas hotspot, *J Geophys Res., 98*, 17,649-17,665, 1993.

Dymond, J, E. Suess, and M Lyle, Barium in deep-sea sediment A geochemical proxy for paleoproductivity, *Paleoceanography, 7*, 163-181, 1992

Dymond, J, R Collier, J McManus, S. Honjo, and S Manganini, Can the aluminum and titanium contents of ocean sediments be used to determine the paleoproductivity of the oceans?, *Paleoceanography, 12*, 586-593, 1997

Emerson, S, Organic carbon preservation in marine sediments, in *The Carbon Cycle and Atmospheric CO_2: Natural Variations Archaen to Present, Geophys Monogr Ser.*, vol 32, edited by E.T Sundquist and W.S Broecker, pp. 78-87, AGU, Washington, D. C., 1985

Emerson, S., and M Bender, Carbon fluxes at the sediment-water interface of the deep-sea. Calcium carbonate preservation, *J Mar Res., 39*, 139-162, 1981.

Emerson, S., R. Jahnke, M. Bender, P Froelich, G. Klinkhammer, C. Bowser, and G. Setlock, Early diagenesis in sediments from the eastern equatorial Pacific, I, Pore water nutrient and carbonate results, *Earth Planet. Sci. Lett., 49*, 57-80, 1980.

Farrell, J.W, and W.L Prell, Climatic change and $CaCO_3$ preservation: An 800,000 year bathymetric reconstruction from the central equatorial Pacific Ocean, *Paleoceanography, 4*, 447-466, 1989.

Farrell, J W, T.F. Pedersen, S E Calvert, and B Nielsen, Glacial-interglacial changes in nutrient utilization in the equatorial Pacific Ocean, *Nature, 377*, 514-517, 1995.

Filippelli, G.M, and M.L Delaney, Similar phosphorous fluxes in ancient phosphorite deposits and a modern phosphogenic environment, *Geology, 20*, 709-712, 1992.

Filippelli, G.M, and M.L. Delaney, Phosphorous geochemistry and accumulation rates in the eastern equatorial Pacific Ocean: Results from Leg 138, *Proc. Ocean Drill. Program, Sci. Results, 138*, 757-767, 1995.

Filippelli, G.M., and M.L. Delaney, Phosphorous geochemistry of equatorial Pacific sediments, *Geochim. Cosmochim. Acta, 60*, 1479-1495, 1996.

Francois, R., S. Honjo, S.J. Manganini, and G.E. Ravizza, Biogenic barium fluxes to the deep sea: Implications for paleoproductivity reconstruction, *Global Biogeochem. Cycles, 9*, 289-303, 1995.

Froelich, P N., M.L. Bender, N A. Luedtke, G.R. Heath, and T. DeVries, The marine phosphorous cycle, *Am J Sci., 282*, 474-511, 1982.

Gill, J, *Orogenic Andesites and Plate Tectonics*, 390 pp, Springer-Verlag, New York, 1981.

Goldberg, E D., and G.O S. Arrhenius, Chemistry of Pacific pelagic sediments, *Geochim Cosmochim. Acta, 13*, 153-212, 1958.

Grundmanis, V, and J W Murray, Aerobic respiration in pelagic marine sediments, *Geochim. Cosmochim Acta, 46*, 1101-1120, 1982

Hammond, D.E., J. McManus, W.M. Berelson, T.E Kilgore, and R.H. Pope, Early diagenesis of organic material in equatorial Pacific sediments: stoichiometry and kinetics, *Deep Sea Res, 43*, 1365-1412, 1996.

Hays, J.D, T. Saito, N.D. Opdyke, and L.H. Burckle, Pliocene-Pleistocene sediments of the equatorial Pacific: Their paleomagnetic, biostratigraphic, and climatic record, *Geol. Soc. Am. Bull, 80*, 1481-1514, 1969.

Hays, J D., J. Imbrie, and N J Shackleton, Variations in the Earth's orbit. Pacemaker of the Ice Ages, *Science, 194*, 1121-1132, 1976.

Herguera, J.C, and W H. Berger, Paleoproductivity from benthic foraminifera abundance: Glacial to postglacial change in the west-equatorial Pacific, *Geology, 19*, 1173-1176, 1991

Herguera, J C, and W H. Berger, Glacial to postglacial drop in productivity in the western equatorial Pacific: Mixing rate vs. nutrient concentrations, *Geology, 22*, 629-632, 1994.

Honjo, S, J Dymond, R.W Collier, and S.J Manganini, Export production of particles to the interior of the Equatorial Pacific Ocean during the 1992 EqPac experiment, *Deep Sea Res., 42*, 831-870, 1995

Imbrie, J, J D Hays, D G Martinson, A McIntyre, A C. Mix, J.J. Morley, N G Pisias, W.L. Prell, and N J Shackleton, The orbital theory of Pleistocene climate Support from a revised chronology of the marine $d^{18}O$ record, in *Milankovitch and Climate, Part 1*, edited by A L. Berger et al., pp. 269-305, D. Reidel, Norwell, Mass., 1984.

Jahnke, R A, D B Craven, and J-F Gaillard, The influence of organic matter diagenesis on $CaCO_3$ dissolution at the deep-sea floor, *Geochim. Cosmochim. Acta, 58*, 2799-2809, 1994.

Joint Global Ocean Flux Study (JGOFS), U. S JGOFS Long Range Plan, *U. S. JGOFS Planning Rep 11*, Washington, D. C, 1990

Knowlton, C.W., Productivity controls on carbonate cycles in the central equatorial Pacific Ocean during the late Pleistocene, M.S. thesis, 94 pp, Univ R I, Narragansett, 1998.

LaMontagne, R.W., R.W. Murray, K.-Y. Wei, M. Leinen, and C.-W. Wang, Decoupling of carbonate preservation, carbonate concentration, and biogenic accumulation: A 400 k. y record from the central equatorial Pacific Ocean, *Paleoceanography, 11*, 553-562, 1996

Loubere, P, Deep-sea benthic foraminiferal assemblage response to a surface ocean productivity gradient. A test, *Paleoceanography, 6*, 193-204, 1991.

Loubere, P, Quantitative estimation of surface ocean productivity and bottom water oxygen concentration using benthic foraminifera, *Paleoceanography, 9*, 723-737, 1994.

Loubere, P., A multiproxy reconstruction of biological productivity and oceanography in the eastern equatorial Pacific for the past 30,000 years, *Mar. Micropaleo., 37*, 173-198, 1999.

Lyle, M, D W. Murray, B.P. Finney, J. Dymond, J M. Robbins, and K. Brooksforce, The record of late Pleistocene biogenic sedimentation in the eastern tropical Pacific Ocean, *Paleoceanography, 3*, 39-59, 1988.

Lyle, M W, F. G Prahl, and M. A Sparrow, Upwelling and productivity changes inferred from a temperature record in the central equatorial Pacific, *Nature, 355*, 812-815, 1992.

Marcantonio, F, N Kumar, M Stute, R.F. Anderson, M A. Seidl, P. Schlosser, and A Mix, A comparative study of accumulation rates derived by He and Th isotope analysis of marine sediments, *Earth Planet Sci. Lett., 133*, 549-555, 1995.

Marcantonio, F., R F. Anderson, M. Stute, N. Kumar, P. Schlosser, and A Mix, Extraterrestrial ^{3}He as a tracer of marine sediment transport and accumulation, *Nature, 383*, 705-707, 1996.

Martin, W.R., M Bender, M. Leinen, and J. Orchardo, Benthic organic carbon degradation and biogenic silica dissolution in the central equatorial Pacific, *Deep Sea Res., 38*, 1481-1516, 1991.

McManus, J., D E. Hammond, W M. Berelson, T.E. Kilgore, D J DeMaster, O.G. Ragueneau, and R W Collier, Early diagenesis of biogenic opal: dissolution rates, kinetics, and paleoceanographic implications, *Deep Sea Res., 42*, 871-903, 1995

McManus, J., et al., Geochemistry of barium in marine sediments: Implications for its use as a paleoproxy, *Geochim. Cosmochim. Acta. 62*, 3453-3473, 1998.

McManus, J., W M. Berelson, D.E. Hammond, and G.P. Klinkhammer, Barium cycling in the North Pacific: Implications for the utility of Ba as a paleoproductivity and paleoalkalinity proxy, *Paleoceanography, 14*, 53-61, 1999.

Mix, A.C., Pleistocene paleoproductivity: evidence from organic carbon and foraminiferal species, in *Productivity of the Ocean: Present and Past*, edited by W.H. Berger, V.S. Smetacek, and G. Wefer, pp. 313-340, John Wiley, New York, 1989.

Mix, A.C., N.G. Pisias, R. Zahn, W. Rugh, C. Lopez, and K. Nelson, Carbon 13 in Pacific deep and intermediate waters, 0-370 ka: Implications for ocean circulation and Pleistocene CO_2, *Paleoceanography, 6*, 205-226, 1991.

Moran, S.B., and R.M. Moore, Temporal variations in dissolved and particulate aluminum during a spring bloom, *Estuarine Coastal Shelf Sci., 27*, 205-215, 1988.

Moran, S.B., and R M Moore, The distribution of colloidal aluminum and organic carbon in coastal and open ocean waters off Nova Scotia, *Geochim. Cosmochim. Acta, 53*, 2519-2527, 1989.

Moran, S B, and R M Moore, Kinetics of the removal of dissolved aluminum by diatoms in seawater: A comparison with thorium, *Geochim. Cosmochim. Acta. 56*, 3365-3374, 1992.

Mudelsee, M., and M. Schulz, The mid-Pleistocene climate transition: Onset of 100 ka cycle lags ice volume build-up by 280 ka, *Earth Planet. Sci. Lett., 151*, 117-123, 1997.

Mudelsee, M., and K Stattegger, Exploring the structure of the mid-Pleistocene revolution with advanced methods of time-series analysis, *Geol. Rundsch., 86*, 499-511, 1997.

Murray, D W, Spatial and temporal variations in sediment accumulation in the central tropical Pacific, Ph. D. thesis, 343 pp., Oregon State Univ., Corvallis, 1987.

Murray, J.W., A U S. JGOFS process study in the equatorial Pacific, *Deep Sea Research, Part II, 42*, 275-903, 1995.

Murray, J.W., A U S JGOFS process study in the equatorial Pacific, *Deep Sea Research, Part II, 43*, 687-1434, 1996

Murray, J W, R Le Borgne, and Y. Dandonneau, A U S JGOFS process study in the equatorial Pacific, *Deep Sea Research, Part II, 44*, 1759-2317, 1997

Murray, R W., and M Leinen, Chemical transport to the seafloor of the equatorial Pacific across a latitudinal transect at 135 W: Tracking sedimentary major, trace, and rare earth element fluxes at the equator and the ITCZ, *Geochim. Cosmochim Acta, 57*, 4141-4163, 1993.

Murray, R W, and M Leinen, Scavenged excess Al and its relationship to bulk Ti in biogenic sediment from the central equatorial Pacific Ocean, *Geochim. Cosmochim. Acta, 60*, 3869-3878, 1996

Murray, R.W., M. Leinen, and A R. Isern, Biogenic flux of Al to sediment in the central equatorial Pacific Ocean: Evidence for increased productivity during glacial episodes, *Paleoceanography, 8*, 651-670, 1993.

Murray, R.W., M Leinen, D.W. Murray, A.C. Mix, and C W. Knowlton, Terrigenous Fe input and biogenic sedimentation in the glacial and interglacial equatorial Pacific Ocean, *Global Biogeochem Cycles, 9*, 667-684, 1995.

Murray, R W, C Knowlton, M. Leinen, A C Mix, and C.H Polsky, Export production and terrigenous matter in the central equatorial Pacific Ocean during interglacial oxygen isotope Stage 11, *Global Planet. Change, 24*, 59-78, 2000.

Orians, K J, and K.W. Bruland, The biogeochemistry of aluminum in the Pacific Ocean, *Earth Planet. Sci Lett., 76*, 397-410, 1986.

Orians, K J., E.A. Boyle, and K.W. Bruland, Dissolved titanium in the open ocean, *Nature, 348*, 322-325, 1990.

Oxburgh, R., The Holocene preservation history of equatorial Pacific sediments, *Paleoceanography, 13*, 50-62, 1998.

Oxburgh, R., and W.S Broecker, Pacific carbonate dissolution revisited, *Palaeogeogr., Palaeoclimatol., Palaeoecol., 103*, 31-39, 1993.

Paytan, A., M. Kastner, and F P Chavez, Glacial to interglacial fluctuations in productivity in the equatorial Pacific as indicated by marine barite, *Science, 274*, 1355-1357, 1996.

Pedersen, T F., Increased productivity in the equatorial Pacific during the last glacial maximum, *Geology, 11*, 16-19, 1983.

Pedersen, T F, M Pickering, J S Vogel, J N Southon, and D.E Nelson, The response of benthic foraminifera to productivity cycles in the eastern equatorial Pacific: Faunal and geochemical constraints on glacial bottom water oxygenation levels, *Paleoceanography, 3*, 157-168, 1988

Pedersen, T.F., B Nielsen, and M. Pickering, Timing of late Quaternary productivity pulses in the Panama Basin and implications for atmospheric CO_2, *Paleoceanography, 6*, 657-677, 1991

Peterson, L.C., and W.L. Prell, Carbonate dissolution in recent sediments of the eastern equatorial Indian Ocean: Preservation patterns and carbonate loss above the lysocline, *Mar. Geol, 64*, 259-290, 1985.

Pisias, N.G, and D.K. Rea, Late Pleistocene paleoclimatology of the central equatorial Pacific: Sea surface response to the southeast trade winds, *Paleoceanography, 3*, 21-37, 1988.

Raymo, M.E., D.W. Oppo, and W. Curry, The mid-Pleistocene climate transition: A deep sea carbon isotopic perspective, *Paleoceanography, 12*, 546-559, 1997.

Rea, D K, N G Pisias, and T. Newberry, Late Pleistocene paleoclimatology of the central equatorial Pacific. Flux patterns of biogenic sediments, *Paleoceanography, 6*, 227-244, 1991.

Schroeder, J O, R W Murray, M Leinen, R.C Pflaum, and T.R. Janecek, Ba in equatorial Pacific carbonate sediment: Terrigenous, oxide, and biogenic associations, *Paleoceanography, 12*, 125-146, 1997.

Smith, C.R., D.J. Hoover, S E. Doan, R.H. Pope, D.J. DeMaster, F.C Dobbs, and M A. Altabet, Phytodetritus at the abyssal seafloor across 10° of latitude in the central equatorial Pacific, *Deep Sea Res., Part II, 43*, 1309-1338, 1996.

Smith, C R, W Berelson, D.J. DeMaster, F C. Dobbs, D Hamond, D J. Hoover, R.H. Pope, and M. Stephens, Latitudinal variations in benthic processes in the abyssal equatorial Pacific: control by biogenic particle flux, *Deep Sea Res., Part II, 44*, 2295-2317, 1997.

Snoeckx, H, and D K Rea, Late Quaternary CaCO3 stratigraphy of the eastern equatorial Pacific, *Paleoceanography, 9*, 341-351, 1994.

Stephens, M.A., and D.C. Kadko, Glacial-Holocene calcium carbonate dissolution at the central equatorial Pacific seafloor, *Paleoceanography, 12*, 797-804, 1997.

Stroobants, N, F Dehairs, L. Goeyens, N. Vanderjeijden, and R. Van Grieken, Barite formation in the Southern Ocean water column, *Mar. Chem., 35*, 411-421, 1991

Taylor, S.R., and S M McLennan, *The Continental Crust: Its Composition and Evolution*, 312 pp, Blackwell, Malden, Mass., 1985

Thompson, P R, and T. Saito, Pacific Pleistocene sediments: Planktonic foraminifera dissolution cycles and geochronology, *Geology, 2*, 333-335, 1974.

Weber, M.E, and N.G. Pisias, Spatial and temporal distribution of biogenic carbonate and opal in deep-sea sediments from the eastern equatorial Pacific: Implications for ocean history since 1.3 Ma, *Earth Planet. Sci. Lett., 174*, 59-73, 1999.

Weber, M.E., M. Wiedicke, V. Riech, and H. Erlenkeuser, Carbonate preservation history in the Peru Basin: Paleoceanographic implications, *Paleoceanography, 10*, 775-800, 1995.

Wei, K-Y, Z.-W Zhang, M.-T. Chen, A.R Isern, C-H Wang, and M. Leinen, Late Quaternary paleoceanography of the central equatorial Pacific: A quantitative record of planktic foraminiferal, isotopic, organic carbon, and calcium carbonate changes, *J. Geol Soc. China, 37*, 475-496, 1994.

Wu, G., and W.H. Berger, Planktonic foraminifera. Differential dissolution and the Quaternary stable isotope record in the western equatorial Pacific, *Paleoceanography, 4*, 181-198, 1989.

Yarincik, K M., Murray R. W., and L. C. Peterson, Climatically controlled eolian and hemipelagic deposition in the Cariaco Basin, Venezuela, over the past 578,000 years: Results from Al/Ti and K/Al *Paleoceanography, 15*, 210-228, 2000.

C Knowlton and M. Leinen, Graduate School of Oceanography, University of Rhode Island, Narragansett, RI 02882 (cknowlto@gso.uri edu; mleinen@gso uri.edu)

A C Mix, Ocean Sciences, Oregon State University, Corvallis, OR 97331. (mix@oce.orst.edu)

R W Murray, Department of Earth Sciences, Boston University, Boston, MA 02215 (rickm@bu edu)

C H Polsky, Department of Chemistry and Biochemistry, Arizona State University, Tempe, AZ 85287

(Received September 20, 1999;
revised July 3, 2000.
accepted July 25, 2000.)